Universidad Zaragoza

1474

Trabajo Fin de Máster

Función de los microARNs del tejido adiposo subcutáneo en la regulación de la esteatosis hepática.

Role of microRNAs from subcutaneous adipose tissue in the regulation of hepatic steatosis.

Autor

José Andrés Castillo Rivas

Directores

Silvia Lorente Cebrián - UNIZAR

José Miguel Arbonés Mainar - IACS

Master in Biophysics and Quantitative Biotechnology

FACULTAD DE CIENCIAS
2024–2025

Acknowledgments

Abstract

Background: Hepatic steatosis arises from excessive triglyceride sythesis in hepatocytes and correlates with the progression of metabolic dysfunction-associated steatotic liver disease (MASLD). Molecules secreted by subcutaneous white adipose tissue (scWAT), such as microRNAs (miRNAs), appear to influence MASLD by regulating key molecular pathways. This study aimed to identify miRNA as a potential biomarkers linked to steatosis in the scWAT of individuals with obesity and varying degrees of hepatic steatosis.

Methods: Subcutaneous white adipose tissue (scWAT) samples were collected from 78 individuals with obesity undergoing bariatric surgery. The patients were categorized into four steatosis groups based on liver fat content: "<5%", "5–33%", "33–66%", and ">66%". Small RNA sequencing data from scWAT were processed with the *nf-core/smrnaseq pipeline* (v2.4.0), and gene expression analysis utilized the *DESeq2* and *isomiRs* R packages.

Results: A total of 374 miRNAs were found to be differentially expressed between patients with obesity with varying degrees of hepatic steatosis. Among these, two miRNAs (*hsa-miR-372-3p* and *hsa-miR-144-3p*) remained significant after multiple test correction. Bioinformatic analysis of predicted target genes revealed their involvement in pathways related to hepatocellular carcinoma and hepatitis B. The *in vitro* essays *hsa-miR-372-3p* mimic show a significance downregulation the mRNA expression of the target gene *ACACA* and *FAS*, however, *hsa-miR-144-3p* inihibitor show no significant results on any of the target genes.

Conclusions: The differential expression of *hsa-miR-372-3p* and *hsa-miR-144-3p* in scWAT suggests that these miRNAs may play a role in the regulation of hepatic steatosis and the progression of MASLD. Their association with hepatocellular carcinoma and hepatitis B pathways underscores their potential relevance to liver pathology. These findings open avenues for research on miRNA profiles as biomarkers or therapeutic targets for MASLD, with a focus on distinguishing simple steatosis from advanced disease.

Table of contents

List of Tables

List of Figures

Chapter 1

Introduction and Antecedents

1.1 Overview of Hepatic Steatosis and Metabolic dysfunction- associated steatotic liver disease

Hepatic steatosis, defined by the excessive accumulation of triglycerides within hepatocytes, results from a wide range of factors that arising from nutritional and metabolic factors, including obesity, insulin resistence, and dysregulated lipid metabolism[1,2]. This excessive accumulation of lipids triggers a harmful mechanism known as "lipotoxicity," characterized by the toxic effects of lipid intermediates on hepatocytes, ultimately leading to cell apoptosis[3]. Lipotoxicity is a critical driver in the progression of metabolic dysfunction-associated steatotic liver disease (MASLD) to metabolic dysfunction-associated steatohepatitis (MASH)[4]. Furthermore, hepatic steatosis is a central feature of steatotic liver disease (SLD), which is categorized into two main subtypes: alcohol-related liver disease (ALD) and MASLD, the latter being the predominant form linked to metabolic dysfunction in the global population[5].

MASLD and its more advanced form, metabolic dysfunction-associated steatohepatitis (MASH), were previously known as nonalcoholic fatty liver disease (NAFLD) and nonalcoholic steatohepatitis (NASH), respectively[4]. MASLD is diagnosed in adults who exhibit hepatic steatosis, identified through imaging techniques, blood biomarkers, or liver histology, in conjunction with being overweight or obese[6], or in the presence of type 2 diabetes mellitus (T2DM) or at least two metabolic risk abnormalities (hypertension, hyperlipidaemia or insulin resistance)[7,8]. Although in many cases it may be asymptomatic in its early stages, this condition can progress to more severe stages such as hepatocellular carcinoma (HCC), depending on its cause[9]. It encompasses a spectrum of liver pathologies ranging from simple hepatic steatosis to metabolic dysfunction-associated steatohepatitis (MASH), which is marked by lobular inflammation and hepatocellular ballooning, potentially progressing to fibrosis and cirrhosis, ultimately leading to liver failure[10].

The prevalence of MASLD is affecting more than a third of the adult population worldwide, making it the most common chronic liver disease globally[11]. Among adults, the prevalence (MASLD) is approximately 30%[12]. MASLD is particularly prevalent in overweight or obese individuals, with a global incidence of approximately 50%, rising to nearly 60% in individuals with type 2 diabetes (T2D)[13].

Over the last 30 years, the global prevalence of MASLD has experienced significant growth, rising from 17.6% in 1990 to 23.4% in 2019, reflecting an average annual increase of approximately

1.0%. As of 2019, it was estimated that there were around 1.66 billion prevalent cases of MASLD worldwide[14]. This condition is widespread, with the highest rates reported in South America (44%), Middle East East and North Africa (36%) and followed by South Asia (33%), South-East Asia (33%), North America and Australia (31%), East Asia (29%), Asia Pacific regions (28%) and Western Europe (25%)[12,15] (Figure 1.1). Approximately one-quarter of the European population is affected by this liver disease[8]. In Europe, the prevalence of NAFLD variates between countries ranging from 5% to 44%[16]. Data from Spain reflect similar rates, indicating a NAFLD prevalence of 25.8% in the adult population[17].
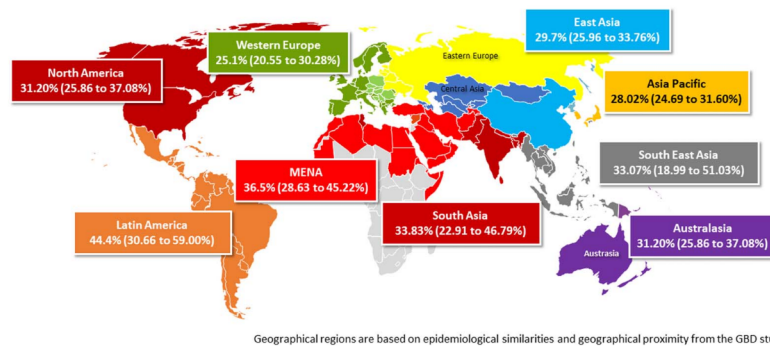
Figure 1.1: Prevalence of MASLD According to Global Regions Data Collected 1990–2019. Image modified from Younossi *et al.*[15]

This growing prevalence of MASLD is closely intertwined with the global rise in obesity and metabolic syndrome, conditions largely influenced by the complex interplay of adipose tissue function and dysfunction. Understanding the role of adipose tissue in metabolic regulation is therefore critical for elucidating the pathophysiology of MASLD.

1.2 Role of Adipose Tissue in Metabolic Regulation

1.2.1 Metabolic and Endocrine Functions of Adipose Tissue

Adipose tissue (AT) is a complex and dynamic organ with both metabolic and endocrine functions[18]. It plays a pivotal role in energy balance, insulin sensitivity, immune responses and overall health[19]. Its role extends beyond simple fat storage, influencing whole-body physiology and contributing to various pathologies, notably obesity and its associated complications like MASLD[20].

1.2.2 Types and Location of Adipose Tissue

Adipose tissue in mammals exists in three primary forms: white adipose tissue (WAT), brown adipose tissue (BAT), and beige or brite (brown-in-white) adipose tissue. Each type is distinguished by its unique functions and cellular composition[21]. WAT primarily stores energy in the form of lipids, while BAT specializes in heat production through the uncoupling of oxidative phosphorylation, a process critical for thermogenesis[22]. Beige AT, a metabolically flexible tissue, can transition between energy storage and thermogenesis depending on physiological needs, highlighting its role in adaptive responses[23] (Figure 1.2). The anatomical distribution of WAT further underscores its functional diversity.

WAT is classified into two major subtypes based its localization and function:

- Subcutaneous white adipose tissue (scWAT), which constitutes over 80% of total body fat and serves as the primary site for long-term energy storage that its located beneath the skin, with its distribution and metabolic activity linked to protective effects on overall metabolic health[24].

- Visceral white adipose tissue (visWAT), which accounts for 10–20% of total body fat in men and 5–10% in women, is more metabolically active, and is strongly associated with adverse health outcomes such as insulin resistance and inflammation. visWAT is located surrounding internal organs such as the liver and intestines[24–26].
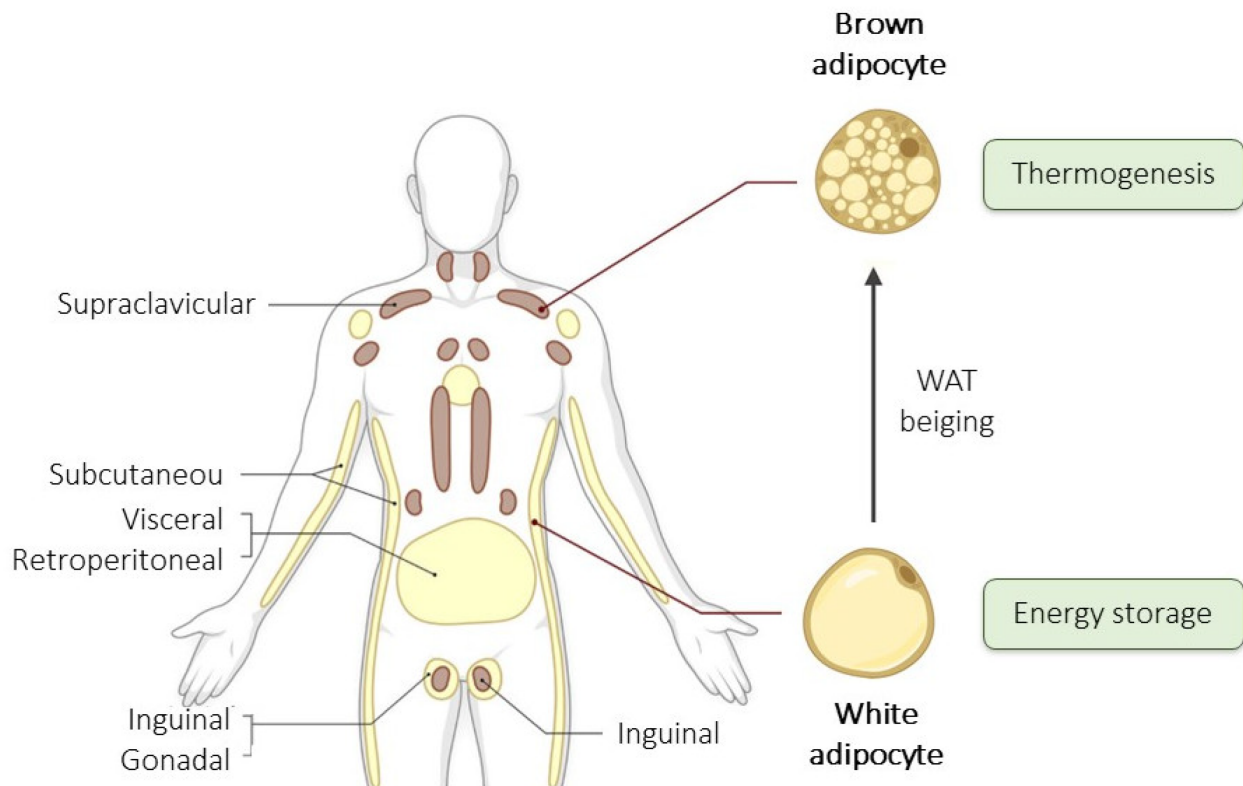
Figure 1.2: Adipose tissue distribution in humans. White adipose tissue (WAT), represented in yellow, is primarily responsible for energy storage, while brown adipose tissue (BAT), in brown, is a thermogenic tissue. Image from Lopez-Yus *et al.*[23]

1.3 Subcutaneous White Adipose Tissue (scWAT)

Subcutaneous White Adipose Tissue (scWAT) is including the upper (deep and shallow abdomen) and lower (gluteofemoral) body areas[27]. Under physiological conditions, scWAT serves as a metabolically inert, long-term triglyceride storage site[28]. Acting as a buffer for excess energy, scWAT protects other organs from ectopic lipid deposition and contributes to specific metabolic benefits[21]. This buffering role allows scWAT to mitigate the impact of excess dietary lipid consumption while also compensating for energy deficits during fasting, starvation, or strenuous exercise[28].

scWAT is composed predominantly of adipocytes, which constitute approximately 50% of its

cellular content[29]. In addition to adipocytes, scWAT includes vascular cells, fibroblasts, adipocyte precursors, multipotent mesenchymal stem-like cells, nerve cells, and immune cells such as macrophages, lymphocytes, eosinophils, and mast cells. These components are embedded within an extracellular matrix that provides structural support[29]. Collectively, these cells secrete a wide array of signaling molecules, including adipokines such as leptin, adiponectin, and resistin, which play essential roles in maintaining metabolic homeostasis[23].

1.4 Metabolic Functions of WAT

The main role of white adipose tissue (WAT) is to manage energy balance by storing and releasing fatty acids (FAs) according to variations in energy availability[23]. Furthermore, WAT produces a range of hormones and cytokines, collectively referred to as adipokines, which are crucial for regulating numerous physiological functions[30].

1.4.1 Lipids Storage and Mobilization

WAT maintains energy balance by storing and releasing fatty acids (FAs), a process controlled by the interplay between lipogenesis and lipolysis. This equilibrium is essential for sustaining energy homeostasis during periods of fasting or exercise[23]. In the Figure 1.3 shows these processes in more detail.

Lipogenesis is the process of synthesizing new lipids from excess glucose or dietary fatty acids. This process occurs in the cytoplasm of adipocytes and is tightly regulated by various hormones and enzymes[31]. Insulin, the key hormone involved in this process, facilitates the uptake of glucose and fatty acids into adipocytes and activates essential enzymes for lipid synthesis, including acetyl CoA-carboxylase (*ACC*) and fatty acid synthase (*FAS*)[32] (Figure 1.3).

Lipolysis, on the other hand, is responsible for breaking down stored lipids in adipose tissue to release energy for peripheral organs. This process is particularly important during fasting or exercise when glucose levels are low, prompting the body to utilize stored fat for energy[33]. Lipolysis is regulated by lipases, which are activated by signals from the sympathetic nervous system, primarily mediated by norepinephrine, with some influence from epinephrine. The primary lipases involved include adipose triglyceride lipase (*ATGL*), hormone-sensitive lipase (*HSL*), and monoacylglycerol lipase (*MGL*)[34] (Figure 1.3).

1.4.2 Endocrine Function

Additionally, WAT secretes various hormones and cytokines, collectively known as adipokines, which play essential roles in regulating multiple physiological processes such metabolic, inflammatory, and immune processes throughout the body[30]. The endocrine function of WAT is influenced by nutritional status, physical activity, hormonal levels, and environmental signals, and is closely related to its metabolic and storage functions[35]. The secretion products are shown in the Figure 1.3.

Current understanding of adipose tissue (AT)-derived adipokines encompasses over 100 proteins that interact with various cells and tissues[23]. Leptin and adiponectin are the most characterized and well-studied adipokines. Leptin, the first adipokine to be discovered, has been shown to influence appetite and energy expenditure, serving as an important feedback mechanism to the brain regarding the size and condition of adipose tissue[36]. In contrast, adiponectin promotes

insulin sensitivity and fatty acid oxidation in skeletal muscle and the liver, contributing to the maintenance of glucose and lipid homeostasis[37].

Additionally, WAT releases extracellular vesicles (EVs), small membrane-bound particles containing various bioactive molecules such as microRNAs (miRNAs), proteins, and lipids. These EVs play a role in maintaining energy homeostasis both locally and systemically[38,39].

The endocrine activity of WAT is influenced by factors such as nutritional status, physical activity, hormonal levels, and environmental signals. Dysregulation of WAT function, as observed in obesity and metabolic disorders, can result in insulin resistance (IR), chronic inflammation, and various metabolic and cardiovascular complications[40,41].
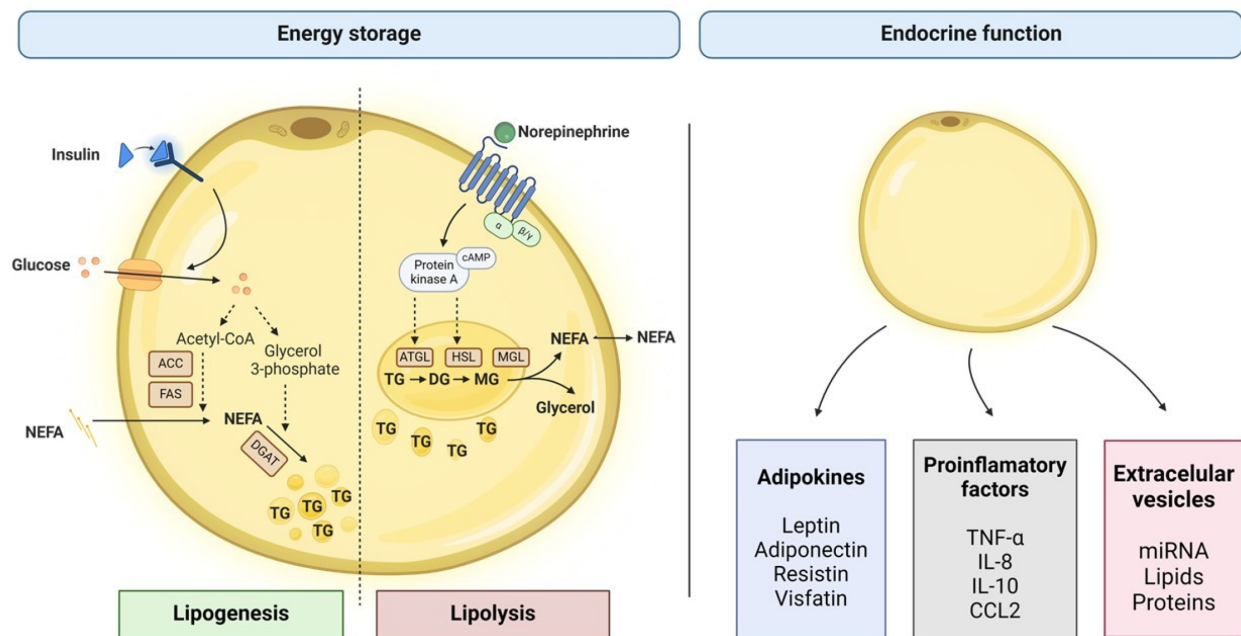
Figure 1.3: Functions of white adipose tissue (WAT). WAT regulates lipogenesis and lipolysis of non-esterified fatty acids (NEFA). WAT also secretes a variety of molecules that play essential roles in the regulation of multiple physiological processes. Image from Lopez-Yus *et al.*[23]. [1]

1.5 Dysregulation of Adipose Tissue and Its Implications

Under prolonged positive energy balance, a failure to expand AT mass via adipocyte hyperplasia (the formation of new adipocytes through precursor differentiation) results in adipocyte hypertrophy (an increase in cell size)[42]. This is a hallmark of AT dysfunction, as enlarged adipocytes have a diminished capacity to store excess dietary energy due to being already saturated with lipids[43,44].

As adipocytes grow in size, they experience increased mechanical stress due to enhanced contact

---

[1]**Abbreviations:** *ACC*, acetyl CoA-carboxylase; *ATGL*, adipose triglyceride lipase; *CCL2*, CC-chemokin-ligand-2; *DGAT*, diacylglycerol-O-acyltransferase; *FAS*, fatty acid synthase; *NEFA*, non-esterified fatty acid; *HSL*, hormone-sensitive lipase; *IL-8*, interleukin 8; *IL-10*, interleukin 10; *IMGL*, monoacylglycerol lipase; *TG*, triglyceride; and *TNF-a*, tumor necrosis factor alpha.

with neighboring cells and components of the extracellular matrix[23]. Additionally, adipocytes face hypoxia, as the hypertrophic expansion of adipose tissue outpaces angiogenesis[45]. Furthermore, hypertrophic adipocytes and damaged cells release pro-inflammatory cytokines, which recruit and activate immune cells. These factors collectively contribute to a chronic low-grade inflammatory state in adipose tissue, significantly impairing its functionality[46].

In individuals with obesity, enlarged adipocytes exhibit partial resistance to the antilipolytic effects of insulin[23]. This increased lipolysis results in elevated levels of free fatty acids (FFAs) in the bloodstream, leading to ectopic lipid deposition and subsequent lipotoxicity. These disruptions can contribute to the onset of systemic insulin resistance, oxidative stress, and the progression of obesity-related comorbidities[47].

The functionality of scWAT is closely linked to body fat distribution[23]. Under pathological conditions, its lipid-storage capacity becomes overwhelmed, leading to hypoxia, infiltration of pro-inflammatory macrophages, and ectopic fat accumulation in other tissues, such as the liver[48]. These alterations disrupt the balance of adipokine secretion, fostering a pro-inflammatory state and systemic insulin resistance, hallmark features in patients with MASLD and related disorders[48].

Understanding the mechanisms underlying scWAT dysfunction highlights the critical role of adipose tissue expandability in metabolic health. The ability of adipose tissue to appropriately expand in response to excess energy intake is crucial for maintaining metabolic homeostasis. When the expansion capacity is compromised, it contributes to the pathogenesis of various metabolic diseases, including MASLD.

1.6   Adipose Tissue Expandability and Liver Fat Deposition

The adipose tissue expandability hypothesis is crucial for understanding MASLD. This hypothesis posits that the body's capacity to store excess calories in subcutaneous adipose tissue (scWAT) is limited and varies between individuals[49]. Once scWAT reaches its maximum storage capacity, adipose tissue can no longer effectively store lipids, leading to the redistribution of lipids to other organs[50]. This results in ectopic fat accumulation, primarily in visceral adipose tissue (visWAT) and the liver, which contributes to insulin resistance and associated metabolic complications through mechanisms driven by lipotoxicity and inflammation[51].

The disparity between energy intake and the storage capacity of adipose tissue is a critical factor in the onset of MASLD. When excessive caloric intake occurs, particularly in conjunction with the limited expandability of subcutaneous adipose tissue (scWAT), it results in fat accumulation in the liver. This hepatic fat buildup, known as steatosis, is a defining characteristic of MASLD and paves the way for additional liver damage[23].

1.6.1   Hepatic Response to Ectopic Fat Accumulation

In MASLD, hepatocytes are the primary cells impacted by ectopic fat deposition. The buildup of triglycerides in hepatocytes, initially serving as a protective mechanism against excess circulating free fatty acids, ultimately results in cellular stress and damage. This fact manifests in various ways:

- *Inflammatory Response*: The accumulation of ectopic fat in the liver triggers an inflammatory response, attracting immune cells and producing pro-inflammatory cytokines. Chronic inflammation induces notable histological changes, that are critical for the progression of

the disease from steatosis to MASH and fibrosis, and may also contribute to hepatocellular carcinoma (HCC)[52].

- *Endoplasmic Reticulum (ER) Stress*: The accumulation of lipids disrupts ER function in hepatocytes, triggering an unfolded protein response that further contributes to cellular stress and apoptosis[53].

- *Oxidative Stress*: When lipid overflow exceeds the capacities of mitochondria and peroxisomes, respiratory oxidation becomes impaired, resulting in the generation of harmful metabolites and excess reactive oxygen species (ROS)[54]. These reactive molecules cause oxidative stress, worsening necro-inflammatory processes in the liver and damaging mitochondria. ROS and oxidized low-density lipoproteins (LDL) activate Kupffer and hepatic stellate cells, leading to collagen deposition and secondary liver fibrosis[55,56].

- *Lipotoxicity*: Increased lipid levels, particularly saturated fatty acids and harmful lipid species such as diacylglycerol (DAG) and ceramide, lead to lipotoxic stress in hepatocytes, causing dysfunction and cell death[57].

- *Altered Metabolism*: In a fatty liver, hepatocytes exhibit changes in carbohydrate and lipid metabolism, often linked to insulin resistance. This exacerbates lipid accumulation and impairs liver function[58].

1.7 miRNAs and Adipose Tissue Regulation

1.7.1 miRNA biology, biogenesis and function

MicroRNAs (miRNAs) are a highly conserved family of small (21–25 nucleotides) noncoding RNAs[59,60]. miRNAs are considered negative regulators of gene expression, functioning by either suppressing translation or promoting mRNA degradation through base pairing with complementary sequences in the 3'-untranslated region (3'-UTR) of protein-coding mRNA transcripts[61]. Notably, mRNA degradation constitutes the primary mechanism of miRNA activity[62]. miRNAs were first identified in *Caenorhabditis elegans* by Victor Ambros and Gary Ruvkun, who were awarded the 2024 Nobel Prize in Physiology or Medicine for their groundbreaking work on miRNAs[63–65].

miRNAs have the ability to regulate hundreds of mRNA targets, and a single mRNA can be influenced by multiple miRNAs[66]. In the human genome, approximately 2,500 miRNAs have been identified[67], with about 60% of protein-coding genes being regulated by miRNAs at the post-transcriptional level[68]. Due to this regulation ability, miRNAs are key regulators within complex genetic pathways, providing a post-transcriptional layer of control over homeostatic and developmental processes[69]. They play critical roles in a wide range of biological functions, including the regulation of the cell cycle, proliferation, lipid metabolism, inflammation, and fibrosis, among others[70]. However, the dysregulation of miRNA has been implicated in the pathogenesis of several many diseases and metabolic disorders, including MASLD[71–74]. Specific miRNAs are known to be differentially expressed in metabolic tissues, including adipose tissue, in response to pathological states[69]. Their potential as biomarkers for disease progression and therapeutic targets has garnered significant interest in recent years[71].

The biogenesis of miRNAs begins with the maturation of miRNAs occurs through a multi-step process that begins with transcription by RNA polymerase II[75,76]. This enzyme synthesizes single-stranded, non-protein-coding RNAs, which can be transcribed either as independent transcripts

(intergenic miRNAs), often containing multiple miRNAs, or derived from the introns of protein-coding genes (intragenic or intronic miRNAs)[69]. The transcription of intergenic miRNAs produces primary miRNAs (pri-miRNAs) with a distinct hairpin or stem-loop structure and extends 1 kb or much longer,[77], resulting in a long primary transcript[78] (Figure 1.4).
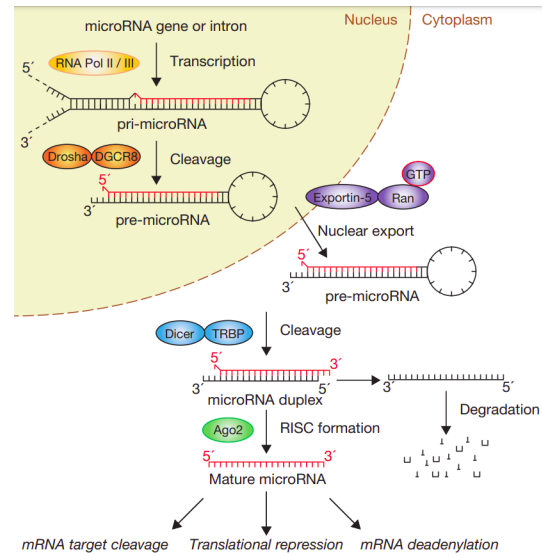
Figure 1.4: Canonical pathway of miRNA biogenesis and processing to mature miRNA. Image from Winter *et al.*[76]

Then the pri-miRNA is cleaved by ribonulease III-type protein Drosha[79] and RNA binding protein DiGeorge Syndrome Critical Region 8 (DGCR8)[80] in the nucleus to produce a ~70 nucleotide long hairpin structure named precursor miRNA (pre-miRNA). Pre-miRNAs are transported to the cytoplasm by exportin-5, where they are cleaved by the ribonuclease III enzyme Dicer in complex with TRBP. This cleavage removes the terminal hairpin structure and generates a ~22-nucleotide miRNA:miRNA* duplex[81].

The selection of one strand of the miRNA:miRNA* duplex is influenced by the thermodynamic stability at the duplex ends[75]. This duplex associates with an Argonaute (AGO) protein to form the RNA-induced silencing complex (RISC). The mature miRNA is generated when the miRNA* strand is removed from the duplex. Generally, the strand with lower thermodynamic stability at its 5' end is preferentially loaded into an Argonaute protein (AGO). Notably, miRNA* is not merely a byproduct of miRNA biogenesis; in many instances, it functions as a regulatory miRNA[82].

The loaded strand, referred to as the guide strand (miRNA), directs the miRNA-induced silencing complex (miRISC) to the mRNA target. In contrast, the unloaded strand, known as the passenger strand (miRNA*), is unwound from the guide strand and subsequently degraded by cellular machinery[83,84].

In addition, the diversity of miRNAs can lead to variations known as isomiRs, which arise from imprecise cleavage by Drosha and Dicer, 3' addition events, RNA editing, or single nucleotide polymorphisms (SNPs)[84,85]. These isomiRs contribute to the functional complexity of the miRNA landscape, further expanding the regulatory potential of miRNAs and highlighting their importance in the intricate mechanisms of gene regulation.

1.7.2   Mechanisms of miRNA-mediated gene regulation

The interaction between miRNAs and their target mRNAs forms a complex miRNA-mRNA interactome, where miRNAs bind to various regions of mRNAs. In the 3' untranslated region (3' UTR), miRNA binding typically induces transcript degradation or translation inhibition. Interactions in the 5' UTR and coding regions can also repress gene expression[86]. Furthermore, miRNA binding to promoter regions may induce transcription, although this mechanism remains poorly understood[83].

The classical mechanism of action of the miRNAs involves inhibiting gene expression by binding to complementary sequences, typically 6–8 nucleotides long, within the 3' untranslated region (3' UTR) of target mRNAs[69]. The miRNA strand loaded into Argonaute (AGO) proteins guides the miRNA-induced silencing complex (miRISC) to miRNA response elements (MREs) on the target mRNA. The outcome of this interaction depends on the degree of complementarity: perfect matches result in transcript degradation, whereas partial complementarity inhibits gene expression either through mRNA degradation or translation repression. Interestingly, some miRNAs can act independently of the miRISC complex. However, the mechanisms underlying these miRISC-free actions are not yet fully understood and warrant further investigation[83,86].

Due to the requirement for only a 6–8 nucleotide complementarity, a single miRNA can potentially target hundreds of mRNAs. Typically, one miRNA targets multiple mRNAs that are interconnected within the same metabolic pathway. This targeting capability allows miRNAs to regulate the expression of numerous other miRNAs, thereby contributing to a complex network of regulatory interactions[87,88]. In fact, most mammalian mRNAs are conserved targets of miRNAs[89]. Bioinformatic tools have become essential for predicting and validating miRNA-target interactions, facilitating the study of miRNA regulatory networks[90,91].

1.7.3   Association of miRNA with Hepatic Steatosis

miRNAs play a critical role in regulating key metabolic pathways in various liver cell types during the transition from steatosis to fibrosis, influencing processes such as lipid metabolism, oxidative stress, inflammation, and fibrosis[73]. Throughout the progression of MASLD, miRNAs have been shown to be involved at every stage of the disease spectrum through diverse regulatory mechanisms[72]. This is of considerable intest providing that they could act as biomarkers of disease prognosis.

Acting as negative posttranscriptional regulators of gene expression, miRNAs also influence the expression of genes involved in lipid metabolism.

Given the critical role of miRNAs in regulating metabolic pathways in the liver, it is essential to explore those specific miRNAs are associated with hepatic steatosis. These miRNAs can be categorized according to their primary effects, allowing for a more detailed understanding of their involvement in this condition

- miRNAs Involved in Lipid Accumulation: *miR-20b* inhibits *PPARα* reducing free fatty acid oxidation and mitochondrial biogenesis, which increases hepatic lipid accumulation[92]. *miR-32* activates sterol regulatory element binding protein-mediated adipogenesis, promoting de novo lipogenesis and liver lipid accumulation[93]. *miR-30a-3p* upregulates lipid metabolism-related proteins and downregulates mitochondrial proteins leading to liver fat accumulation[94] . *miR-130b-5p* was found upregulated in MASLD murine models, increasing

hepatic lipid accumulation via the IGFBP2-dependent AKT pathway[95]. *miR-451a* regulates THRSP, reducing triglyceride accumulation in the liver[96].

- miRNAs Implicated in Insulin Resistance: *miR-188* targets *ATG12*, negatively regulating hepatic glucose and lipid metabolism, which worsens steatosis and insulin resistance[97]. *miR-27* disrupts insulin/AKT signaling by targeting *PDPK1* and *PIK3R1*, leading to insulin resistance[98]. *miR-30b* induces ER stress by targeting *SERCA2b*, contributing to insulin resistance[99]. *miR-144* targets Irg1, suppressing the production of itaconate and enhancing *SDH* and *FH* activity, which reduces fumarate levels, inhibits *NRF2* activation, and impairs the antioxidant response, worsening oxidative stress and metabolic complications in obesity[100].

- miRNAs Regulating Fatty Acid Oxidation: *miR-100* regulates directly *CD36*, reducing fatty acid uptake in hepatocytes and downstream lipid metabolic mediators[101].*miR-376b-3p* targets *FGFR1*, increasing fatty acid oxidation and improving hepatic lipid accumulation[102].

- miRNAs Associated with Endoplasmic Reticulum (ER) Stress: *miR-26a* mitigates high-fat diet-induced ER stress and steatosis by targeting $eIF2\alpha$[103].

- miRNAs Modulating Inflammatory and Fibrotic Pathways: *miR-222* regulates mitophagy in hepatic stellate cells (HSCs) by targeting *PINK1*, contributing to fibrosis in MASH[104,105]. *miR-146a*: Suppresses fibrosis and improves hepatic lipid/glucose metabolism by targeting *WNT1* and *WNT5a*[106,107].

- miRNAs Affecting Lipogenesis and Lipolysis: *miR-199a-5p* reduces *MST1*, modulating hepatic lipogenesis and lipolysis[108]. *miR-103-3p* targets *ACOX1*, promoting hepatic steatosis and worsening MASLD[109]. Furthermore, *miR-802* inhibits *AMPK* expression, promoting NAFL/MASH[110].

- Regulatory Insights: Part of the *miR-17-92 cluster*, exacerbates steatotic changes by regulating *CYP7A1* signaling[111]. Aditionally, *miR-132* is involved in lipid homeostasis by suppressing multiple regulatory transcripts[112].

Table 1.1: miRNAs and Their Molecular Targets in Hepatic Steatosis

miRNA	Molecular Target	Effect	Reference
miR-20b *miR-30a-3p* *miR-32* *miR-130b-5p* *miR-451a*	$PPAR\alpha$, *ACC*, *p-GSK-3β* , *FASN*, *CPT1*, *p-AMPK*, *UCP2*, *IGFBP2*, *INSIG1*, *THRSP*	Changes in hepatic lipid accumulation	[92–96]
miR-27 *miR-30b* *miR-144* *miR-188*	*ATG12*, *PDPK1*, *PIK3R1*, *SERCA2b*, Irg1	Implicated in insulin resistence	[97–99]
miR-100 *miR-376b-3p*	*CD36*, *FGFR1*	Regulating Fatty Acid Oxidation	[101,102]
miR-199a-5p *miR-103-3p* *miR-802*	*MST1*, *ACOX1* *AMPK*	Affecting Lipogenesis and Lipolysis:	[108–110,113]

miRNA	Molecular Target	Effect	Reference
miR-222 *miR-146a*	*ACOX1, PINK1, MED1, WNT1, WNT5a*	Modulating Inflammator and Fibrotic Pathway	[104–107]
miR-17	*CYP7A1*	Steatotic changes	[111]
miR-26a	*eIF2α*	Endoplasmic Reticulum stress and high-fat diet-induced steatosis	[103]
miR-132	*SIRT1, P300, PTEN, CYP2E1, FOXO3*	Lipid homeostasis	[112]

1.7.4   miRNAs as Biomarkers Based on Omics Sciences

The arrival of omics technologies has been essential in advancing precision medicine by providing an unprecedented ability to analyze complex biological systems. However, their contribution to the identification of clinically relevant biomarkers is often indirect, primarily due to the challenges associated with managing and interpreting largre datasets[114]. According to the World Health Organization, a biomarker is defined as "any substance, structure, or process that can be measured in the body or its products and that can influence or predict the incidence or outcome of a disease''[115,116]. Omics technologies, such as genomics, transcriptomics, and metabolomics, generate massive datasets that enable the discovery of molecules potentially associated with disease incidence, prognosis, or therapeutic response. This discovery process requires subsequent validation using established analytical techniques such as FISH, RT-PCR, PCR, or immunoaffinity assays before biomarkers can be approved for clinical use[114]. Despite these complexities, the integration of omics data with clinical insights continues to unlock valuable opportunities for disease characterization and management.

The ability of a biomarker to provide a detailed characterization of a disease allows the stratification of patients into well-defined groups for tailored management and treatment, which forms the foundation of precision medicine[117]. Biomarkers can be categorized into four groups: diagnostic biomarkers, which identify a specific health condition in a patient; prognostic biomarkers, which help to chart the progression of a disease; predictive biomarkers, which suggest the expected response to a specific treatment; and predisposition biomarkers, which assess the likelihood of developing a particular illness[114,117].

Among emerging biomolecules, miRNAs have gained significant attention as potential biomarkers[117]. These small non-coding RNA molecules are involved in critical cellular processes such as lipid metabolism, inflammation, and fibrosis, suggesting that they can serve as monitoring tools for various diseases, including metabolic dysfunction-associated diseases[72,118]. miRNAs are primarily found in the cytoplasm, their presence has also been confirmed in circulatory system and various bodily fluids, including saliva and urine[83]. This occurs due to processes such as cellular lysis, apoptotic body release, or active secretion. Their detection in biological fluids highlights their potential as non-invasive biomarkers for diseases such as MASH and MASLD[119]. Their detection in biological fluids highlights their potential as non-invasive biomarkers for diseases such as MASH and MASLD[119]. Circulating miRNAs can be categorized into three main types: (1) those enclosed within microvesicles, exosomes, or apoptotic bodies; (2) protein-associated miRNAs

bound to RNA-binding proteins such as AGO2 or HDL; and (3) free-floating miRNAs [[83];[66]; ;[120]]. miRNAs have indeed been identified in adipocytes, which are considered a primary source of exosomal miRNAs[118,121]. This diversity underscores their biological and clinical significance.

A critical advantage of circulating miRNAs is their remarkable stability in extracellular environments. Their association with proteins or vesicles protects them from degradation by RNases, allowing for reliable detection[122]. Additionally, miRNAs exhibit high sensitivity and specificity in disease detection, and their measurement allows multiplex analyses, which further enhances diagnostic precision. However, challenges remain, such as variability in detection methods, the need for standardized protocols, and low miRNA abundance in some cases[66]. Addressing these barriers through advancements in absolute quantification methods, exosome-targeting strategies, and improved extraction techniques will be crucial for translating miRNA research into clinical applications[120].

Emerging evidence highlights the role of miRNAs in the pathogenesis of MASLD and its progression to MASH and HCC. Dysregulated miRNA expression in liver tissue and circulation has been linked to key pathways, including lipid metabolism, inflammation, fibrosis, and cell proliferation[123]. For instance, miR-122 and miR-34a have been consistently identified as dysregulated in patients with MASLD, correlating with disease severity and progression[119]. These findings suggest that miRNAs may serve as diagnostic and prognostic biomarkers and even as therapeutic targets. However, knowledge gaps persist regarding the exact mechanisms by which miRNAs contribute to disease progression, particularly in MASH-related hepatocarcinogenesis. Further research is required to elucidate these pathways and establish causality.

In summary, miRNAs represent a transformative class of biomarkers with significant potential to reshape precision medicine. Their stability in extracellular conditions, combined with their presence in readily accessible fluids, makes them ideal candidates for non-invasive diagnostics and monitoring. Specific miRNA profiles may enable patient stratification and personalized treatment strategies, optimizing therapeutic efficacy while minimizing adverse effects. Advances in omics technologies, coupled with innovations in bioinformatics and analytical platforms, are expected to accelerate the integration of miRNAs into clinical practice.

The present study contributes to this growing field by combining bioinformatics analyses, in vitro models, and genetic manipulation to investigate miRNAs associated with hepatic steatosis in patients with obesity. By identifying miRNAs involved in lipogenesis, lipolysis, and β-oxidation, this research aims to uncover novel tools for preventing and treating metabolic disorders such as MASLD and MASH. Furthermore, the potential to use these miRNAs as non-invasive biomarkers or therapeutic targets represents a significant advancement in personalized medicine. This multi-dimensional approach not only expands our understanding of metabolic biology but also holds promise for direct clinical applications, ultimately improving the care of patients with obesity and associated liver diseases.

Chapter 2

Hypothesis and Objectives

2.1 Hypothesis

The main hypothesis of this study is that microRNAs (miRNAs) derived from subcutaneous adipose tissue might play a key role in regulating metabolic processes involved in the development and progression of hepatic steatosis. These miRNAs can alter fundamental metabolic pathways by modulating genes associated with lipid metabolism in human hepatocytes.

More specifically, it is proposed that:

- miRNAs secreted or expressed in the subcutaneous adipose tissue of patients with obesity, are involved in intercellular communication that affects lipid accumulation in the liver, contributing to the development of hepatic steatosis.

- Bioinformatic analysis of RNAseq data might identify differentially expressed miRNAs in the subcutaneous adipose tissue of patients with obesity, associated with key metabolic pathways related to lipogenesis, lipolysis, and β-oxidation.

- The experimental modulation of specific miRNAs in *in vitro* cellular models of human hepatocytes, through overexpression or inhibition strategies, can reveal their functional role in processes related to hepatic steatosis.

- The functional characterization of these miRNAs enable their use as potential biomarkers or therapeutic targets for the prevention and treatment of obesity-associated hepatic steatosis.

2.2 Main objective

To identify the function of microRNAs (miRNAs) expressed in subcutaneous adipose tissue in the regulation of metabolic processes involved in the development of hepatic steatosis, with the aim of these miRNAs could contitute potential biomarkers and therapeutic targets for obesity management.

2.3   Specific Objectives

1. To analyze RNAseq data from subcutaneous adipose tissue of obese patients obtained from the FATe cohort (ADIPOFAT).

2. To identify a set of differentially expressed miRNAs associated with metabolic pathways involved in lipogenesis, β-oxidation, and lipolysis related to hepatic steatosis.

3. To establish in vitro cell models of human hepatocytes to study the function of candidate miRNAs.

4. To modify the expression of specific miRNAs through transfection with synthetic analogs in an in vitro model of steatosis.

5. To evaluate the expression of key genes related to lipogenesis, lipolysis, and β-oxidation in miRNA-transfected hepatocytes.

6. To explore the potential of identified miRNAs as biomarkers or therapeutic targets for the treatment of obesity and its associated disorders.

Chapter 3

Methodological Framework

3.1   Study Population

The analyzed data originates from the FATe cohort[124], a longitudinal study of patients with obesity undergoing bariatric surgery at Miguel Servet University Hospital (HUMS, Zaragoza, Spain). For this research, 78 patients with varying degrees of adiposity were selected based on subcutaneous adipose tissue (scWAT) samples, which are registered at the regional Biobank (Biobanco Aragón) and approved by the CEICA ethics committee. Patients with alcohol or drug abuse, autoimmune diseases, chronic inflammatory conditions, or infectious diseases (HIV, HBV, HCV) were excluded during the screening process. The FATe cohort is characterized by a range of clinical and demographic variables, including sex, age, body mass index (BMI), steatosis, metabolic dysfunction-associated steatohepatitis (MASH), hepatocytic ballooning, lobular inflammation, diabetes, hyperlipidemia, and metabolic dysfunction-associated steatotic liver disease (MASLD).

3.2   Collection and characterization of subcutaneous white adipose tissue

White adipose tissue biopsies (~3 cm³) from the subcutaneous depot were obtained during laparoscopic bariatric surgery using a bipolar/ultrasonic device (Thunderbeat). The samples were extracted through a 12 mm trocar (Applied Medical) inserted into the left hypochondrium. An experienced pathologist evaluated pathological features such as steatosis, lobular inflammation, hepatocellular ballooning, and fibrosis according to the criteria established by the Nonalcoholic Steatohepatitis Clinical Research Network ([125]).

3.3   RNA isolation

Total RNA was extracted from frozen biopsies of subcutaneous white adipose tissue (scWAT) and cell cultures using TRIzol (#T9424, Sigma Aldrich) following the manufacturer's instructions. For lysing adipose tissue samples, 1 ml of TRIzol was added *per* sample in a homogenizer, while for cell cultures, 1 ml of TRIzol was used *per* 10 cm² of the culture plate, along with a scraper. The resulting cell lysates or tissue disaggregates were transferred to a vial and incubated for 5 minutes at room temperature to dissociate nuclear components. Subsequently, 0.2 ml of 100% chloroform

per ml of TRIzol was added. The mixture was shaken vigorously, incubated for 15 minutes at room temperature, and then centrifuged for 15 minutes at 12,000 g and 4 ºC.

Following centrifugation, three distinct phases were formed. The aqueous phase, which contained the ribonucleic acids, was collected, and 0.5 ml of 100% isopropanol was added to precipitate the RNA. This mixture was unified, incubated on ice for 10 minutes, and then centrifuged at 12,000 g for 15 minutes at 4 ºC. Afterward, the supernatant was carefully decanted, and the RNA pellet was resuspended in 1 ml of 75% ethanol for washing. The pellet was homogenized and centrifuged at 7,500 g for 5 minutes at 4 ºC. The supernatant was discarded, and the pellet was allowed to dry for 10 minutes at room temperature. Finally, the RNA was resuspended in DEPC-treated water. To eliminate any genomic DNA contamination, all RNA samples were treated with RNase-Free DNase (Life Technologies). The concentration and purity of the RNA were assessed by measuring absorbance at 260/280 nm and 260/230 nm using a Nanodrop 2000 (Thermo Fisher Scientific Inc.) and Qubit 4 Fluorometer (Thermo Fisher Scientific Inc.). The quality of the extracted RNA was visualized using an agarose gel.

3.4   RNA Sequencing

RNA integrity was evaluated using the RNA Integrity Number (RIN) on the Agilent 2200 TapeStation with the RNA ScreenTape assay. Stranded mRNA libraries were prepared with the Novogene NGS RNA Library Prep Set (PT042), which included mRNA isolation using poly-T oligo-attached magnetic beads, cDNA synthesis, adapter ligation, and PCR amplification. Libraries that passed quality control checks were sequenced (2x150 bp) on the Illumina Novaseq X Plus platform.

3.5   Analysis of small RNA-seq Data with *nf-core/smrnaseq*

For the analysis of small RNA sequencing (sRNA-seq) data, version 2.4.0 of the *nf-core/smrnaseq* pipeline[126] was used, which is specifically designed for the automated processing of miRNAs data.

3.5.1   Execution of the *nf-core/smrnaseq* Pipeline

The installation of *nf-core/smrnaseq* was carried out following the instructions provided by the authors in *nf-core*[127], available at https://nf-co.re/smrnaseq/2.4.0 .

To ensure the proper installation and execution of the pipeline, the following key components were installed beforehand:

1. *Nextflow*: Version 24.04.4 of Nextflow was used, following the detailed instructions at https://nf-co.re/usage/installation.

2. *Java Runtime Environment (JRE)*: Version 11.0.25 of the Java Runtime Environment was installed, as it is required for compatibility with Nextflow and the *nf-core/smrnaseq* pipeline.

To ensure reproducibility and streamline the pipeline execution, one of the available Docker containers was utilized. These containers provide the necessary instructions and configurations required to run the pipeline. The configuration is specified at runtime using the `profile` argument. For this analysis, the Docker image *nf-core/smrnaseq*, available at Docker Hub, was employed.

The pipeline was executed on a server with 8 CPUs, 16 GB of RAM, and a Linux operating system. The following command was used in the terminal, which configures the main options, including the reference genome, input data, and output file location:

```
nextflow run nf-core/smrnaseq -r 2.4.0
-profile docker,ci
--genome GRCh38
--input '/home/joshoacr13/Documentos/TFM/nfcore-smrnaseq/input/samples.csv'
--fasta 'https://github.com/nf-core/test-datasets/raw/smrnaseq/reference/genome.fa'
--mirtrace_species 'hsa'
--outdir /home/joshoacr13/Documentos/TFM/nfcore-smrnaseq/workdir
-resume -c /home/joshoacr13/Documentos/TFM/nfcore-smrnaseq/nextflow_memory.config
--filter_contamination
```

The pipeline was executed three times to accommodate the large number of samples, processing 26 samples *per* run.

3.5.2 Description of the Parameters Used

- `-profile docker,ci`: Runs the pipeline inside a Docker container to ensure reproducibility and sets up a continuous integration (CI) profile.

- `--genome GRCh38`: Specifies the human genome (version GRCh38) as the reference for sequence mapping.

- `--input`: Provides the path to the CSV file containing metadata and the paths to the FASTQ files.

- `--fasta`: URL to the FASTA file of the reference genome.

- `--mirtrace_species hsa`: Defines the species as Homo sapiens (hsa) for miRNAs analysis with miRTrace.

- `--outdir`: Sets the working directory for the processed results.

- `-resume`: Allows continuation of a previous analysis without restarting from the beginning.

- `-c`: Specifies a custom configuration file (nextflow_memory.config) to adjust resource usage.

- `--filter_contamination`: Enables the contamination filtering.

3.5.3 Analysis Workflow and Tools Used

The *nf-core/smrnaseq* pipeline is performed following the next steps:

1. **Quality Control** An initial quality assessment of the raw reads was conducted using *FastQC* (version 0.12.1)[128]. Additionally, 3' adapter trimming was performed using *fastp* (version 0.23.4)[129], followed by quality and length filtering. A second quality assessment of the trimmed reads was conducted with *FastQC*.

2. **miRNA Quality Control**: A more specific quality control process for miRNA sequencing was implemented, whereby samples that failed to meet the minimum quality thresholds established by *miRTrace* (version 1.0.1)[130] were excluded from further analysis. This tool incorporates the following steps to ensure the integrity and reliability of the data:

- **Verify Read Length Distribution**: The majority of reads fell within the expected range of 18–24 nucleotides, indicative of high-quality small RNA data.
- **Identify Contaminants**: Potential contaminants such as tRNA, rRNA, and other non-target molecules were flagged.
- **Taxonomic Classification**: Reads were classified taxonomically to ensure that most sequences originated from the organism of interest (*Homo sapiens*).

3. **miRNAs Quantification**:

- **Alignment**: The filtered reads were aligned against mature miRNA sequences in the miRBase database using *Bowtie1* (version 1.3.1)[131]. Unmapped reads were aligned against "hairpin" sequences to identify miRNA precursors.
- **Post-Alignment Processing**: *SAMtools* (version 1.16.1)[132] was used to process the mapping results.

4. **IsomiR Annotation**: The collapsed reads were processed with *mirtop* (version 0.4.28)[133] to identify miRNA variants (isomiRs).

5. **Analysis and Visualization of Results**: The overall pipeline metrics, encompassing quality assessments, mapping statistics, and expression analysis results, were consolidated and summarized using *MultiQC* (version 1.25.1)[134]. Visualization of the results was performed using the *ggplot2* package in R[135], which facilitated the creation of clear and informative graphical representations.

3.6   Differential expression analysis according to steatosis using *DEseq2*

For the differential expression analysis, the R statistical software[136], version 4.4.1 (2024-06-14) (https://cran.r-project.org/), was used. This analysis was performed using the RStudio integrated development environment (IDE)[137], version 2023.12.0+369, designed for Ubuntu Jammy (https://www.rstudio.com/).

The script used to perform the differential expression analysis is available in the file "miRNA_steatosis.qmd" which can be accessed at the following link: https://github.com/joshoandres13/miRNAs.

The analysis began by loading essential R packages: *tidyverse* (version 2.0.0)[138] for data manipulation, *isomiRs*[139] (version 1.32.1) for analyze isomirs and miRNAs from sRNA-seq, *DESeq2* (version 1.44.0)[140] for differential expresion analysis, *org.Hs.eg.db* (version 3.19.1)[141] for gene annotation.

3.6.1   Data Preparation

Metadata were imported, and sample identifiers were stablished as row names. The variable *Steatosis* is categorized in four distinct groups. Isomirs count data were subsequently obtained where rows represent the identified isomiRs and columns correspond to the experimental samples.

Using isomirs count data and metadata, an object of class IsomirDataSeq was created. This object enables efficient management of information derived from small RNA sequencing studies, streamlining differential expression analyses and facilitating the interpretation of biological findings.

3.6.2   Filtering and Processing of isomiRs

The filtering process enables the grouping of isomiRs into distinct categories, associating them with a single variant of a miRNA. This grouping is essential for ensuring consistency and accuracy in differential expression analyses. To reduce technical noise and highlight biologically meaningful signals, a stringent filtering criterion was applied: only isomiRs with a minimum of 20 counts in at least 40 samples were retained.

3.6.3   Differential expression in scWAT

In this study, the *DESeq2* package was used to perform differential expression analysis on scWAT samples with varying degrees of liver steatosis. The *DESeq2* object was configured using the Likelihood Ratio Test (LRT), enabling the analysis to account for all four steatosis categories: <5% (no steatosis), 5–33% (mild steatosis), 33–66% (moderate steatosis), and >66% (severe steatosis). This approach allowed for a comprehensive assessment of gene expression changes across the entire spectrum of steatosis progression.

3.6.3.1   Testing for differential expression

The criteria for identifying significant differentially expressed miRNAs across the steatosis categories involved applying a false discovery rate (FDR) cutoff of less than 0.05. Following the identification of significant miRNAs, the expression patterns of the selected miRNAs were further analyzed by representing their normalized counts in boxplots across the four steatosis groups. This approach enabled the observation of expression variations of these miRNAs across different steatosis degrees, offering insights into their potential roles in steatosis progression. Differences between steatosis groups were evaluated using the Kruskal-Wallis test

3.7   Target mRNA Selection and Validation Using *multiMiR*

The selected miRNAs were used for the identification of mRNA targets through the *multiMiR* bioinformatics package[142,143], version 2.4.0 in R. *multiMiR* facilitates a systematic search and annotation of miRNA targets, providing functional analysis to elucidate biological mechanisms. For this analysis, only validated interaction data were utilized.

3.7.1   Filtering Parameters

The validated target table provided by *multiMiR* was used during the selection process. Key columns included:

1. **database**: Source database of validated interactions, such as *miRTarBase*, *TarBase*, or *miRecords*.
2. **mature_mirna_id**: Standard format identifier for the miRNA.
3. **target_symbol**: Target gene symbol.
4. **experiment**: Experimental methods used for validation, including luciferase assays, Western blot, or qRT-PCR.
5. **support_type**: Level of experimental support, such as "Functional MTI" (miRNA-mRNA functional interaction).
6. **pubmed_id**: References to PubMed articles reporting the interaction.
7. **type**: Specifies whether the interaction is "validated" or "predicted."

3.7.2   Selection Criteria

To ensure reliable results, databases were filtered according to update criteria and the following selection parameters:

- Databases up-to-date at the time of analysis were prioritized (*miRTarBase* and *TarBase*).

- Only interactions classified as "validated" were included.

- Interactions backed by robust experimental methods, such as luciferase assays or Western blot, were prioritized.

- Interactions with functional support ("Functional MTI") and verifiable references in PubMed were selected.

This approach ensured the identification of mRNA targets with high reliability and experimental backing, facilitating the analysis of potential regulatory functions of the studied miRNAs.

3.7.3   Functional Analysis

To explore the biological functions associated with the validated target genes, an enrichment analysis was performed using the *KEGGREST* package[144] in R. Gene symbols for validated target genes associated with selected miRNAs were extracted using *multiMiR* previously, with duplicates removed to ensure a unique gene list. The Entrez IDs of these genes were mapped to specific metabolic pathways in KEGG, using parameters that controlled the false discovery rate (FDR) with the Benjamini-Hochberg method and significance cutoff values for `qvalue` and `pvalue` set at 0.05. The results included a bar plot displaying the top 5 significantly enriched KEGG pathways, highlighting their statistical significance and the number of genes associated with each pathway. This analysis provided insights into key metabolic pathways and biological processes involving miRNA-regulated target genes.

3.8   Functional validation of miRNAs

3.8.1   Cell Culture and Transfections with miRNA Mimics

The human hepatoma HepG2 cell line (American Type Culture Collection, ATCC® HB-8065™; Manassas, VA, USA) was cultured in an incubator at 37 ºC and 5% CO_2 using high-glucose Dulbecco's Modified Eagle Medium L-GlutaMAX (DMEM) (Gibco, Thermo Fisher Scientific Inc., Waltham, MA, USA) supplemented with 10% fetal bovine serum (FBS; Gibco, Thermo Fisher Scientific Inc., Brazil). Experiments were carried out when the cells reached 70-80% confluence.

For the experiments, HepG2 cells were plated at a density of 100,000 cells per well in 12 well-plates for gene expression assays, in DMEM high-glucose (1 g/L) L-GlutaMAX supplemented with 10% FBS.

HepG2 cells were reverse-transfected with Lipofectamine RNAiMAX Reagent (Thermo Fisher Scientific Inc.) and 50 nM of the following mirVana™ synthetic miRNAs (Thermo Fisher Scientific Inc.): a scramble sequence as a negative control (mirVana™ miRNA Mimic, Negative Control #1), negative control (mirVana™ miRNA Inhibitor, Negative Control #1), *miR-144-3p* ($5' - UACAGUAUAGAUGAUGUACU - 3'$; assay ID H11051), and *miR-372-3p* ($5' - AAAGUGCUGCGACAUUUGAGCGU - 3'$; assay ID MC10165). The miRNA mimics were diluted in Opti-MEM I Reduced Serum Medium (Gibco, Thermo Fisher Scientific Inc.) and added

to the wells according to the manufacturer's instructions. Following this, Lipofectamine was added to the wells containing the diluted miRNA mimics and incubated for 15 minutes at room temperature to form miRNA mimic–lipofectamine complexes. HepG2 cells diluted in DMEM with 10% FBS were then plated into the wells. The cells were incubated for 24 hours to assess transfection efficiency. To induce lipid accumulation and simulate steatosis[145], HepG2 cells were treated with oleic acid 24 hours after miRNA mimic transfections, mixed in DMEM GlutaMAX-I supplemented with 10% FBS, at a final concentration of 0.5 mM used to mimic hepatic steatosis, which reflects the physiological range of free fatty acids[146].

HepG2 cells were frozen on dry ice and stored at -80 °C until RNA extraction. Cells used for miRNA expression analyses were washed previously with phosphate-buffered saline (PBS) to completely remove potential unabsorbed miRNA mimics.

3.8.2 Gene Expression Analyses

mRNA expression was evaluated in HepG2 cells transfected with miRNA mimics for 48 h. RNA was reverse transcribed using PrimeScript Reverse Transcriptase (Takara Bio), with 100 ng of RNA utilized for each reaction in a total volume of 10 μl. The process was carried out using an Applied Biosystems 2720 Thermal Cycler, following this protocol: 10 minutes at 25 °C, 2 hours at 37 °C, and finally, 5 minutes at 85 °C. The cDNA product were amplified using Quantitative-real time PCR (qPCR) in a total reaction volume of 15 μl with SYBR Select Master Mix (Applied Biosystems), to which 0.5 μl of gene-specific primers at a concentration of 10 μM was added. The primers utilized are detailed in Table 3.1 qPCR was performed on a StepOnePlus system (Applied Biosystems) with the following protocol: an initial step at 95 °C for 10 minutes, followed by 40 cycles of 15 seconds at 95 °C and 1 minute at 60 °C, concluding with 15 seconds at 95 °C, 1 minute at 60 °C, and a final 15 seconds at 95 °C. The gene β-actin was used as a housekeeping control to normalize gene expression levels ($\triangle Cq$). Comparisons between gene expression levels after miRNA mimic transfections vs. scramble-sequence-transfected cells (negative control) were established using the the $2 - \triangle\triangle CT$ method, determining relative gene expression[147].

Table 3.1: Primers designed for qPCR mRNA gene expression analysis

Gene Name	Forward Primer (5'→ 3')	Reverse Primer (5'→ 3')
ACCA	AGGTGCCTAGAGGGTTGAAGA	TCGGCCCTGCTTTACTAGGT
ATGL (PNPLA2)	TGGAGACTGAGGAGAACAAG	ATCCCTGCTTGCACATCTCT
DGAT2	AGTGGCAATGCTATCATCATCGT	TCTTCTGGACCCATCGGCCCCAGGA
FAS	AAGGACCTGTCTAGGTTTGATGC	TGGCTTCATAGGTGACTTCCA
PPARG	AGATGACAGCGACTTGGCAAT	ACTCAGGGTGGTTCAGCTTC
ACTB-2	ACCGAGCGCGGCTACAG	CTTAATGTCACGCACGATTTCC

Abbreviations: *ACCA* (Acetyl-CoA Carboxylase Alpha), *DGAT2* (Diacylglycerol O-Acyltransferase 2), *FAS* (Fatty Acid Synthase), *PNPLA2* (Patatin-like phospholipase domain-containing protein 2), *PPARG* (Peroxisome Proliferator Activated Receptor Gamma).

3.9   Statistical Analysis

The results are expressed as median [interquartile range] and number of cases (%). Pairwise group comparisons for continuous variables were calculated using Student's t-test for variables with a

Gaussian distribution and the Mann–Whitney U test for data that do not follow this distribution. Categorical variables were analyzed using the chi-square test.

The data obtained from the gene expression experiments were analyzed to determine the statistical significance of the differences observed between the experimental groups treated with synthetic miRNAs and the negative controls. The results are presented as the percentage of relative regulation (fold change) with respect to the negative control, expressed as percentages (mean ± standard error of the mean, SEM). The fold change was calculated by dividing the gene expression of each sample by the mean expression in the negative control. A Student's t-test for independent samples was used to evaluate the differences in the expression of the target genes. Statistical significance was set at $p < 0.05$.

Chapter 4

Results

4.1 Phenotypic Characterization

Table 4.1 describes the phenotypical features of FATe patients selected for this study. This cohort encomprises 78 subjects (24% males; 76% females), aged between 22 to 61 with obesity as regards of BMI levels of 46.11 ± 6.13 kg/m². These patients had an overall presence of general variables/descriptors of metabolic syndrome features of particular interest those related to liver/hepatic status (steatosis, lobular inflammation and the prevalence of associated metabolic diseases). According to the hepatic steatosis scale, 35.9% of patients had less than 5% liver fat, indicating a normal or minimal steatosis state. A total of 32.1% exhibited mild steatosis (5–33%), while 25.6% showed moderate fat accumulation (33–66%). Only 6.4% of patients presented severe steatosis (>66%), with no significant differences between men and women ($p= 0.818$).

Regarding lobular inflammation, most patients (66.7%) had no lobular inflammation, while 24.4% exhibited fewer than two foci per microscopic field, and 3.8% showed severe inflammation (>4 foci). Hepatocyte ballooning analysis revealed that 74.4% of patients did not display significant damage, although 9.0% showed severe ballooning.

Among most prevalent comorbidities, 26.9% of patients were diagnosed with diabetes, and 34.6% presented hyperlipidemia, with the latter being significantly more prevalent in men (63.2%) compared to women (25.4%, $p= 0.006$). Additionally, 15.4% of patients were classified with metabolic dysfunction-associated steatohepatitis (MASH), although this proportion showed no statistically significant differences between genders ($p= 0.249$). Collectively, these data highlight the heterogeneity in the clinical characteristics of the cohort, emphasizing the complexity of the metabolic relationship between obesity and liver disease in this cohort.

4.2 Quality Control (QC) and reads preprocessing

All QC results from the various steps in the *nf-core/smrnaseq* pipeline are summarized in the following figures and tables. The evaluation of samples, both before and after processing, was conducted using *fastp*, a rapid tool designed for preprocessing RNA sequencing data. This tool includes features for adapter trimming, quality filtering, and report generation, making it essential for assessing sample quality. Overall, Table 4.2 presents a descriptive analysis that includes key metrics related to the sequencing data.

Table 4.1: Clinical characteristics of the FATe cohort

Characteristic	Overall (n=78)	Female (n=59)	Male (n=19)	p
Age (years) median	47.03 [13.75]	46.53 [13]	48.58 [14]	0.408
Body Mass Index (kg/m²) median	46.11 [8.70]	45.68 [8.76]	47.42 [8.70]	0.284
MASLD Activity Score Category (%):				0.510
- 0	22 (28.2)	16 (27.1)	6 (31.6)	
- 1	16 (20.5)	13 (22.0)	3 (15.8)	
- 2	17 (21.8)	14 (23.7)	3 (15.8)	
- 3	9 (11.5)	7 (11.9)	2 (10.5)	
- 4	9 (11.5)	7 (11.9)	2 (10.5)	
- >= 5	5 (6.4)	2 (3.4)	3 (15.8)	
Hepatic Steatosis Scale (%):				0.818
- < 5%	28 (35.9)	21 (35.6)	7 (36.8)	
- 5-33%	25 (32.1)	20 (33.9)	5 (26.3)	
- > 33-66%	20 (25.6)	15 (25.4)	5 (26.3)	
- > 66%	5 (6.4)	3 (5.1)	2 (10.5)	
Hepatocytic ballooning Category (%):				0.489
- None	58 (74.4)	45 (76.3)	13 (68.4)	
- Few cells	13 (16.7)	10 (16.9)	3 (15.8)	
- Many cells	7 (9.0)	4 (6.8)	3 (15.8)	
Lobular Inflammation Category (%):				0.596
- No foci	52 (66.7)	41 (69.5)	11 (57.9)	
- < 2 foci/200x	19 (24.4)	14 (23.7)	5 (26.3)	
- 2-4 foci/200x	4 (5.1)	2 (3.4)	2 (10.5)	
- > 4 foci/200x	3 (3.8)	2 (3.4)	1 (5.3)	
Diabetes:				1.000
- Yes (%)	21 (26.9)	16 (27.1)	5 (26.3)	
- No (%)	57 (73.1)	43 (72.9)	14 (73.7)	
Hyperlipidemia:				0.006
- Yes (%)	27 (34.6)	15 (25.4)	12 (63.2)	
- No (%)	51 (65.4)	44 (74.6)	7 (36.8)	
Metabolic dysfunction-associated:				0.249
- MASH (%)	12 (15.4)	7 (11.9)	5 (26.3)	
- Non-MASH (%)	66 (84.6)	52 (88.1)	14 (73.7)	

Description: Data are presented as number of cases (Differences between groups were tested with the Mann–Whitney U test and chi-square test. *BMI*: Body Mass Index (kg/m²), *MASH:* Metabolic dysfunction-associated steatohepatitis.

Table 4.2: Descriptive statistics of the analyzed metrics with fastp

	Mean	sd	Median	Minimum	Maximum	Range
% Duplication	98.30513	0.68	98.45	94.31	99.09	4.78
Reads After Filtering (M)	25.23152	5.67	25.82	1.51	35.47	33.96
% GC content	46.71982	1.68	46.43	43.26	50.89	7.63
% PF	99.02358	1.21	99.36	90.13	99.76	9.63
% Adapter	99.38240	0.35	99.45	96.96	99.62	2.66

Description: *% Duplication*: Duplication rate before filtering, *Reads After Filtering:* Total reads after filtering in million, *% GC content:* GC content after filtering, *% PF:* Percent reads passing filter, *% Adapter:* Percentage adapter-trimmed reads

The metrics obtained from the fastp analysis provide a detailed overview of the preprocessing performance across the samples. The percentage of duplicated reads before filtering was notably high, with a mean of 98.31% (±0.68), a median of 98.45%, and a range between 94.31% and 99.09%. After filtering, the number of reads retained per sample averaged 25.23 million (±5.67M) suggesting a reasonable amount of reads obtained, with a median of 25.82M and a range from 1.51M to 35.47M.

The GC content showed consistency across the samples, with an average of 46.72% (±1.68), a median of 46.43%, and a range between 43.26% and 50.89%. The percentage of pass-filtered (PF%) reads was high, with an average of 99.02% (±1.21), reaching a maximum of 99.76%, as shown in Figure 4.1.
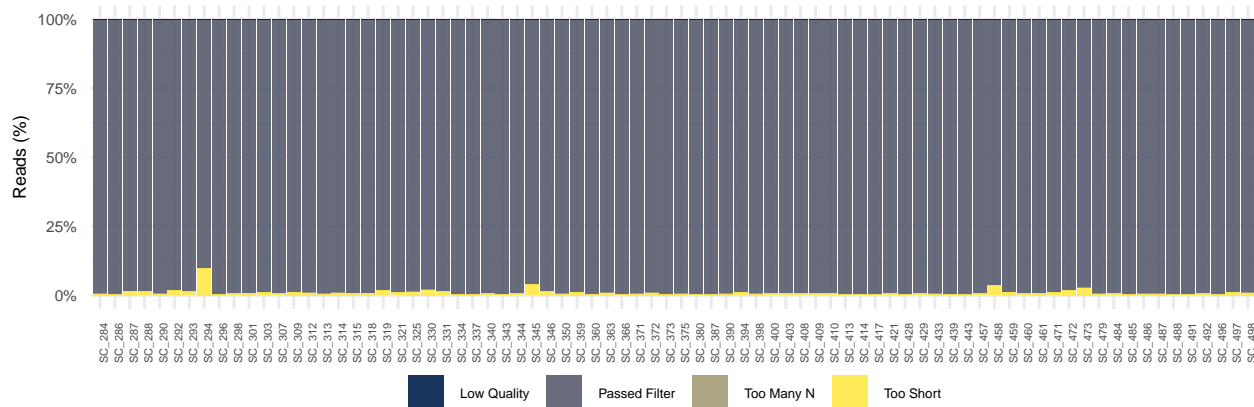
Figure 4.1: Fastp: Filtered Reads

The adapters used in library construction, specifically the *Illumina Universal Adapter* type, are optimized for the amplification and sequencing of diverse sample types. The adapter trimming was highly effective, achieving a mean success rate of 99.38% (±0.35) with a range from 96.96% to 99.62%. (Table 4.2). In line with these findings, Figure 4.2 illustrates the adapter content before and after processing with *fastp*, where the mean trimming percentage of 0.05 ± 0.06% for scWAT samples indicates that adapters were effectively removed from all samples. These results confirm the efficiency of the preprocessing steps, ensuring that high-quality reads were retained while effectively eliminating low-quality sequences and adapters.

A

B
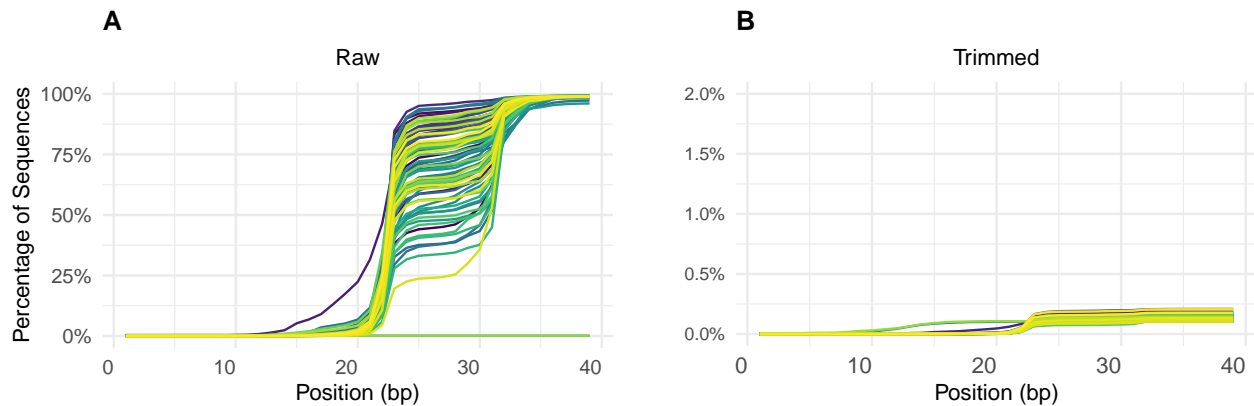
Figure 4.2: Adapters Content (%) across all bases before (A) and after (B) using *fastp* (version 0.23.4)

Figure 4.3 shows the analysis of the mean quality value of sequences across all bases, both before (*A*) and after (*B*) processing with *fastp*, it is evident from that the sequences from all samples consistently fall within an acceptable quality range, with mean Phred scores exceeding 30. This indicates a high base-calling accuracy, with an error probability of less than 0.1%, ensuring robust data integrity throughout the process.

However, there is a noticeable drop in quality towards the extremes of the readings, particularly at position 31 bp. This decline can be attributed to the effects of adapter trimming in smRNA-seq. Even though adapters have been removed, if they were present at the end of the sequence, their trimming may result in reduced quality for the subsequent bases. Bases near the adapter might have lower quality, leading to a set of bases that, while technically valid, originate from a lower-quality region. Additionally, it is common in smRNA-seq to encounter contaminants from various sources, such as rRNA or tRNA, which introduce background noise and can further diminish the quality of the readings obtained.

The Figure 4.3 illustrates the metric of the average quality value of each sequence across all samples. Before processing with *fastp* (*C*), the Phred scores consistently exceed 30, with most samples achieving scores around 35. This indicates that the average sequence quality is optimal, ensuring high reliability and low error rates. However, after trimming (*D*) a slight decrease in both Phred scores and read counts is observed. This reduction in the number of reads is expected after strict preprocessing with *fastp*, especially if contaminated or low-quality reads were present.

In Figure 4.3 (*E*), prior to trimming, the GC content distribution does not follow a normal pattern. Multiple peaks are observed, probably due to the presence of adapters, which typically have a fixed GC content that generates specific peaks. Additionally, since this is a *small RNA-seq* experiment, contamination from rRNA or tRNA is common, as these molecules often have a different GC content compared to other small RNAs. After processing with *fastp* (*F*), the GC content decreases, indicating that most of these contaminant sequences have been removed, leaving of reads with anomalies. This remaining may correspond to sequences that are difficult to classify or contaminants that are not easily eliminated by *fastp*.

Additionally, no issues with the presence of ambiguous bases (Ns) are detected in any of the samples before and after trimming. Figure 4.3 (*G* and *H*).
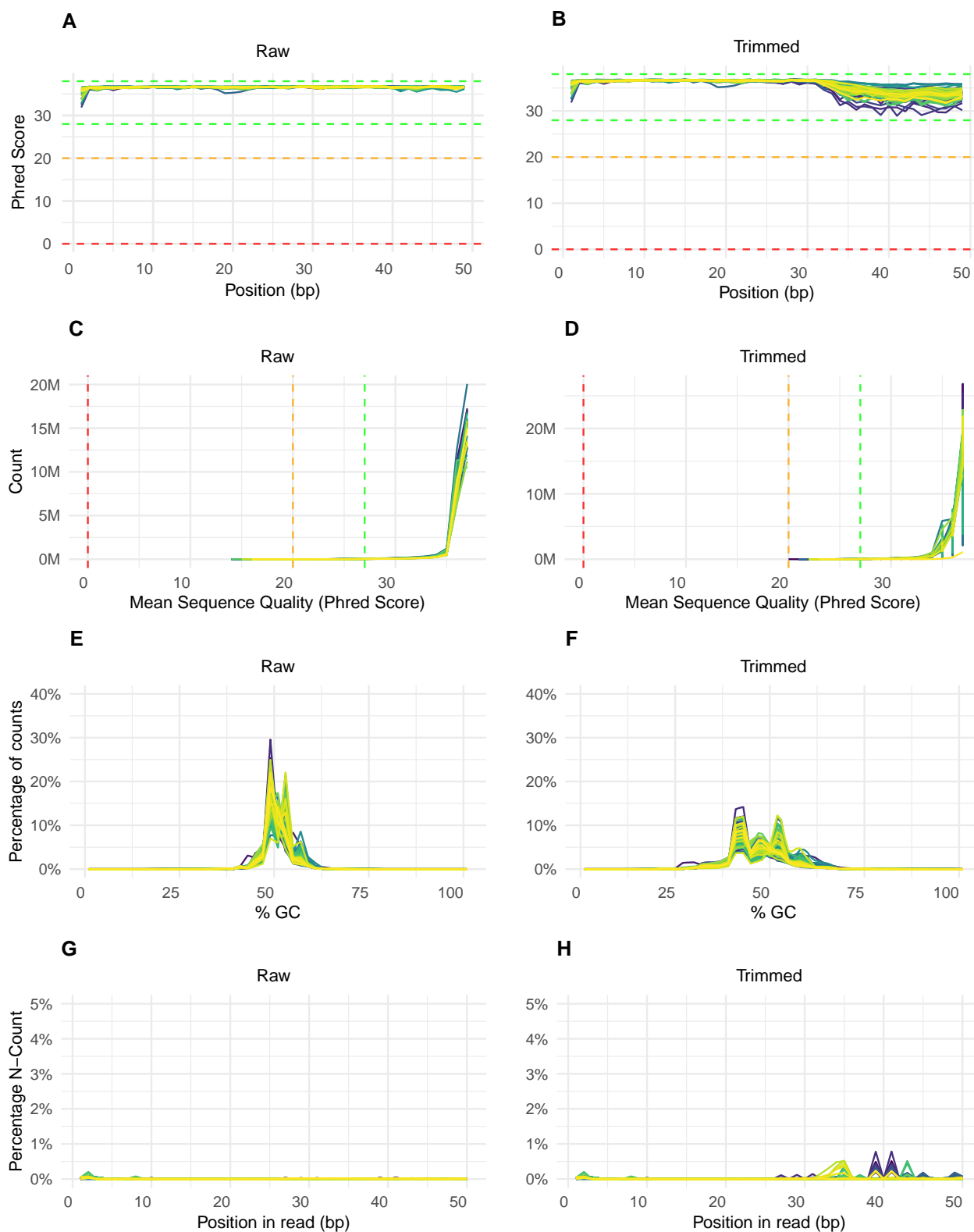
Figure 4.3: Quality Control Analysis. *A* and *B*: Mean quality values of sequences across all bases after ('Trimmed') and before ('Raw') using fastp (v0.23.4); *C* and *D*: Per Sequence Quality Scores across all bases after ('Trimmed') and before ('Raw') using fastp; *E* and *F*: Per Sequence GC Content Raw after ('Trimmed') and before ('Raw') using fastp; *G* and *H*: Read N content after ('Trimmed') and before ('Raw') using fastp.

However, the distribution of sequence lengths is irregular in the samples Figure 4.4. After trimming, the majority of sequences cluster around a length of 20-25 nucleotides, although a smaller subset of sequences with lengths between 29-32 nucleotides is also observed. This indicates the presence of different types of small RNAs. Generally, miRNAs are found in the range of 20-24 bp, with a peak at 22 bp potentially indicating an abundant population of miRNAs. In contrast, tRNAs can vary in length but are commonly found at lengths that may include higher peaks, such as at 31 bp. This may reflect the presence of tRNAs derived from the degradation of double-stranded RNA or transposons.
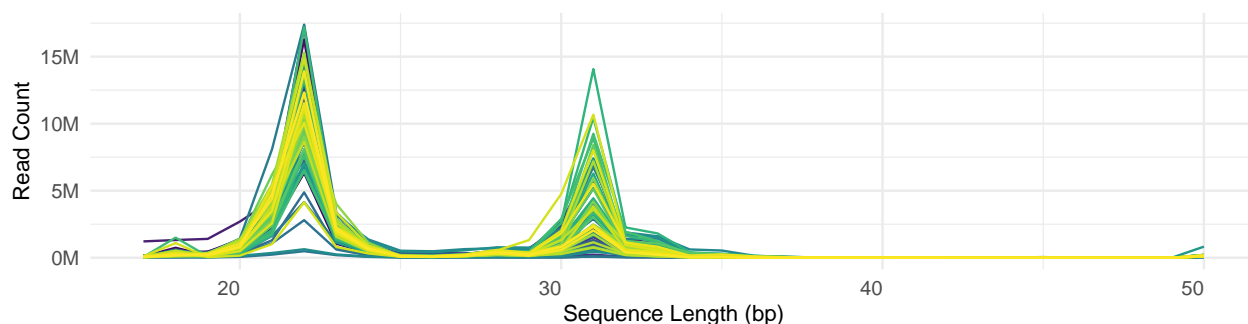
Figure 4.4: FastQC: Sequence Length Distribution

In the Figure 4.5 shows the total number of reads *per* sample is around 25 million, both in Raw and Trimmed, with means of 25.47 and 25.23 million, respectively. The interquartile ranges (IQR) of these measurements are similar, approximately 4.2 million, reflecting a high consistency among the samples.

Regarding duplicate reads, they dominate the data, with means of 25.10 million in Raw and 24.95 million in Trimmed, and an IQR of about 4.2 million in both conditions. This indicates that more than 90% of the sequences are duplicated, a high value but expected in sRNA-seq samples, given the nature of the short reads of 20 to 24 nucleotides.

In contrast, unique reads are significantly less frequent, with means of 0.38 million in Raw and 0.28 million in Trimmed. The interquartile ranges for these measurements are also low, around 0.13 million in Raw and 0.10 million in Trim.
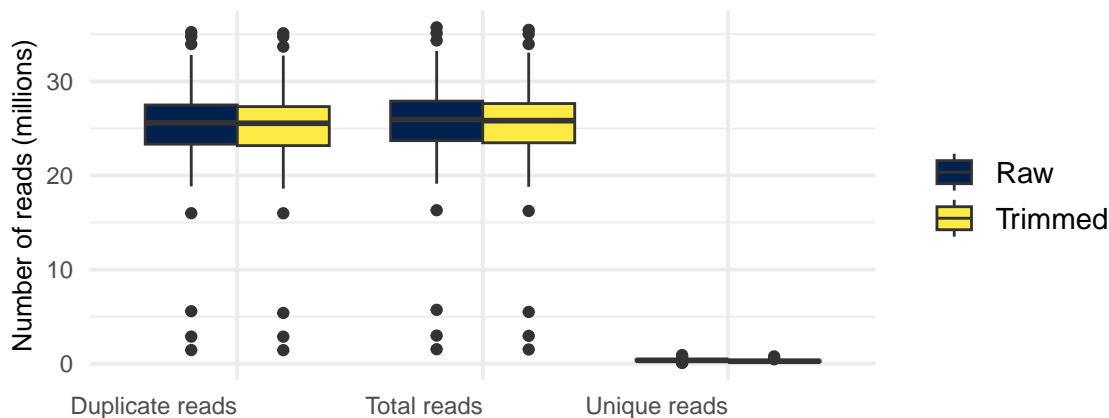
Figure 4.5: Number of reads from small RNA-seq. Total reads before and after trimming of adapters

4.3 miRNA Quality Control

The *nf-core/smrnaseq* pipeline performs a quality analysis specific to sRNA-seq data using *miRTrace*. This analysis assesses sequencing quality, identifies the presence of miRNA, and filters out unwanted sequences such as tRNA, rRNA, or Illumina artifacts. Additionally, it detects clade-specific miRNA profiles based on a comprehensive catalog of previously identified miRNA families.

In the annotation step Figure 4.6, the mapped reads against reference databases revealed that a mean of 65.06% of analyzed sequences per sample corresponded to miRNA precursors, with a range of 22.51% to 91.77%. Other categories included 21.16% tRNA sequences, 9.16% unknown sequences, 4.55% rRNA sequences, and 0.05% artifacts.
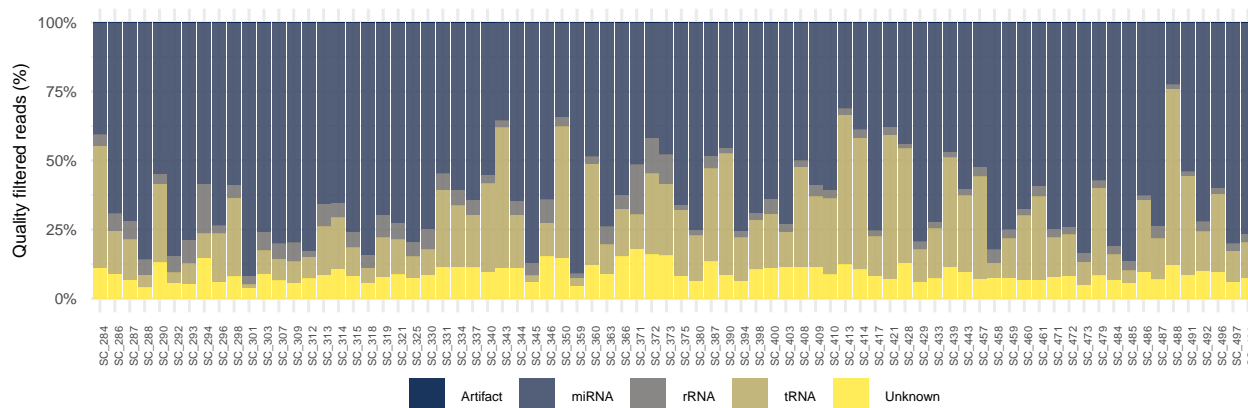
Figure 4.6: *miRTrace* (v1.0.1) Analysis: RNA Categories

During the contamination assessment step Figure 4.7, mapping miRNA precursor sequences against the clade-specific miRNA catalog showed that a mean of 94.14% of analyzed sequences belonged to the human category, with a range of 67.21% to 99.94%. Minor contributions from other clades, such as Rodentia (2.07%), Dicots (2.73%), Insects (0.58%), and Monocots (0.38%), were detected at low proportions. These identifications could result from contamination, such as incorrect index assignment during sample demultiplexing.
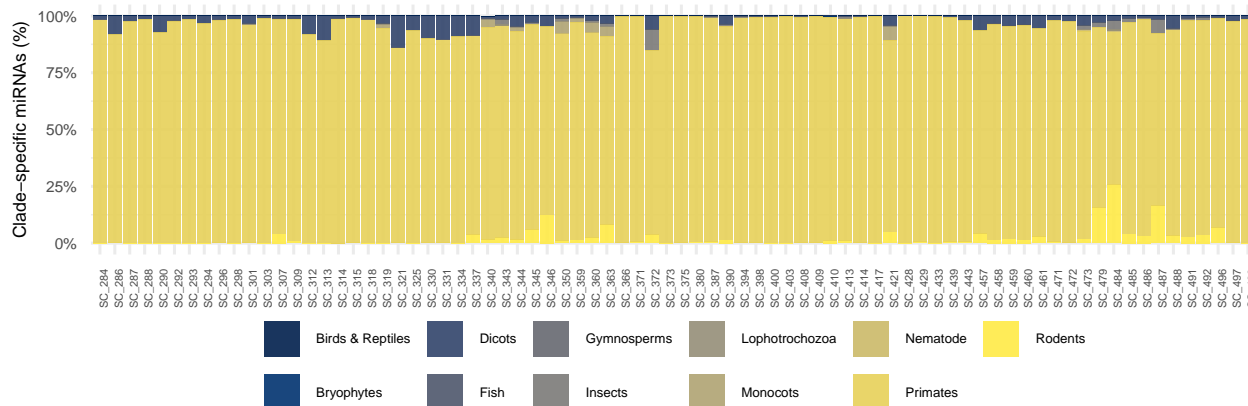
Figure 4.7: *miRTrace* (v1.0.1) Analysis: Contamination Check

4.4   miRNA Quantification

In this step of the *nf-core/smrnaseq pipeline*, the alignment of reads is conducted sequentially against databases of mature miRNAs, precursor miRNAs, and a combined database of both. These alignments enable the identification and quantification of miRNAs. The statistics obtained for mature miRNAs, precursor miRNAs, and the combination of both against the reference genome are presented in Table 4.3. On average, 52.07% of the mature miRNAs were mapped, with a range between 17.72% and 79.75%.

For precursor miRNAs, an average of 32.33% of sequences were identified, ranging from 6.31% to 68.83%. Subsequently, the reads of mature and precursor miRNAs were aligned against a reference genome, not for miRNA identification and quantification but as a quality control for the sequences. In this regard, the mean percentage of aligned reads was around 43% of the total reads. Across the sample set, minimum values of 10.28% and maximum values of 73.31% were observed. For more details, the metrics for each sample can be found in https://github.com/joshoandres13/miRNAs.

Table 4.3: Descriptive statistics of alignment with samtools of all samples. *TM*: Mean of Total Mapped (reads); *TU*: Mean of Total Unmapped (reads): *Mean M*: Mean Mapped (%); *Max M*: Max Mapped (%); *Min M*: Min Mapped (%)

Group	TM	TU	Mean M	Max M	Min M
mature	13166950	12194855	52.07	79.75	17.72
mature_hairpin	3644435	8836242	32.33	68.83	6.31
mature_hairpin_genome	4334118	4565712	43.87	73.31	10.28

4.5   IsomiR Annotation

Mirtop (v0.4.28) was used for the annotation of miRNAs and isomiRs. In Figure 4.8, the *mean isomiR read counts* are presented, which refer to an average calculation that helps to describe how the reads of isomiRs are distributed within a dataset. Among the annotated isomiR sequences per sample, the *reference miRNA* accounts for 96.51%, with ranges varying from 88.70% to 98.13%. On the other hand, the distributions of isomiR variants are as follows: *3' Isoform* (1.36%), *3' Addition* (1.23%), *5' Isoform* (0.64%), *SNVs in the Central Offset Region* (0.05%), *SNVs in the Central Region* (0.06%), *Supported SNVs in the Central Region* (0.05%), and *SNV in Seed Region* (0.05%), all of which are below 1.40%.
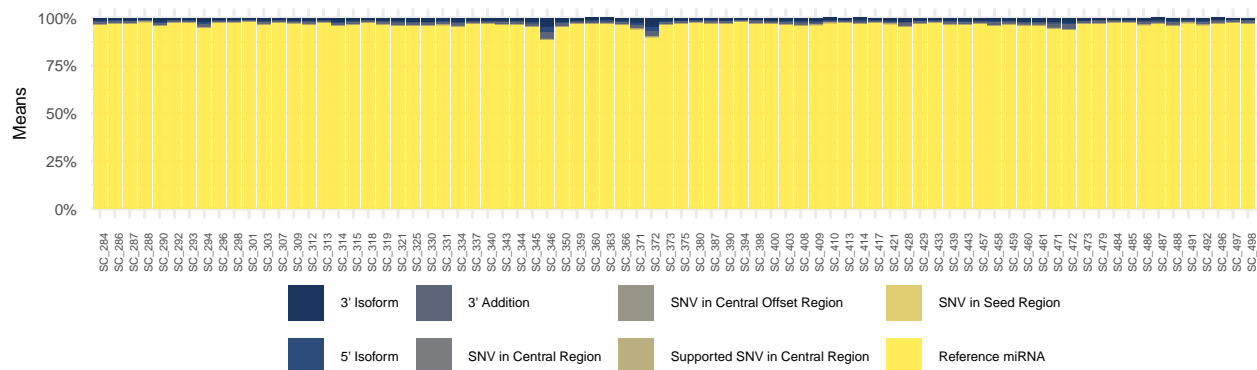
Figure 4.8: Annotation of miRNAs and isomiRs with *mirtop* (v0.4.28): Mean isomiR read counts

4.6 Differential expression analysis

Differential expression analysis is a bioinformatics and statistical technique used to identify genes, proteins, or other biomolecules that exhibit significant differences in expression levels between two or more biological conditions. For this analysis, the sequences of miRNAs of reference were used, as annotated in the previous analysis.

Under the hood of *DESeq2*, we applied the *regularized logarithm* (*rlog*) transformation for normalization, which incorporates a prior on the sample differences[148]. This step is crucial because the standard logarithmic transformation can be sensitive to low expression values, whereas *rlog* addresses this issue by introducing regularization that helps stabilize variability between samples. This method facilitates seamless integration into subsequent analyses, as demonstrated in Figure 4.10, which shows a total of 374 miRNAs were found to be expressed differentially in the overall cohort when patients (samples) were categorized by sex and steatosis.

Since we were primarily interested in the transcriptional changes that may precede the initiation of the steatosis process, we focused on contrasting individuals across different levels of steatosis. In this experimental scenario, the goal is to identify miRNAs that are expressed differentially at various levels of steatosis. In our differential expression analysis using *DESeq2* with the LRT model, we initially identified 169 miRNAs as upregulated and 205 downregulated in the subcutaneous white adipose tissue (scWAT) of individuals according their steatosis degree. Comparing these four groups and applying a false discovery rate (FDR) cutoff of less than 0.05, the number of statistically siginificant differentially expressed miRNAs was greatly reduced to 2 (Figure 4.9). Of these, we found *hsa-miR-372-3p* is upregulated and *hsa-miR-144-3p* is downregulated (Table 4.4).

Table 4.4: Differentially expressed miRNAs in subcutaneous white adipose tissue (scWAT). *FDR* : False Discovery Rate

	log2FoldChange	pvalue	FDR
hsa-miR-144-3p	-3.319	p< 0.0002	0.04
hsa-miR-372-3p	1.085	p< 0.0002	0.04
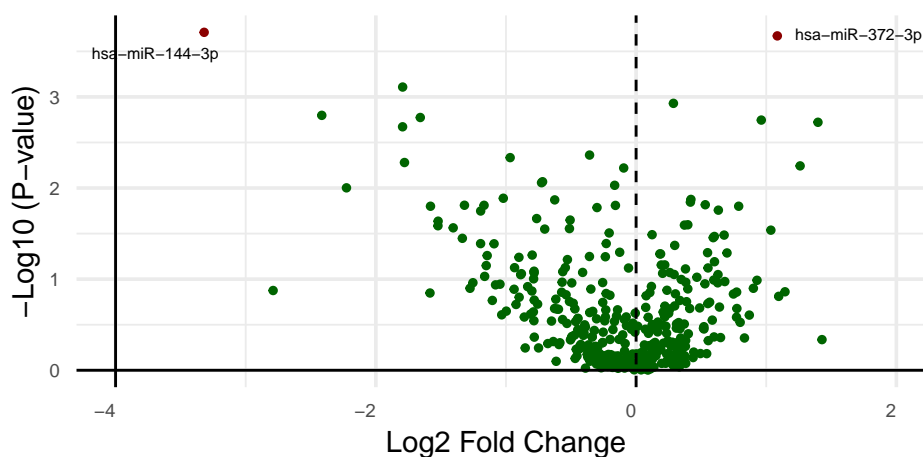
Figure 4.9: Plot showing differentially expressed miRNAs (red) in subcutaneous white adipose tissue (scWAT) according to the four groups of steatosis
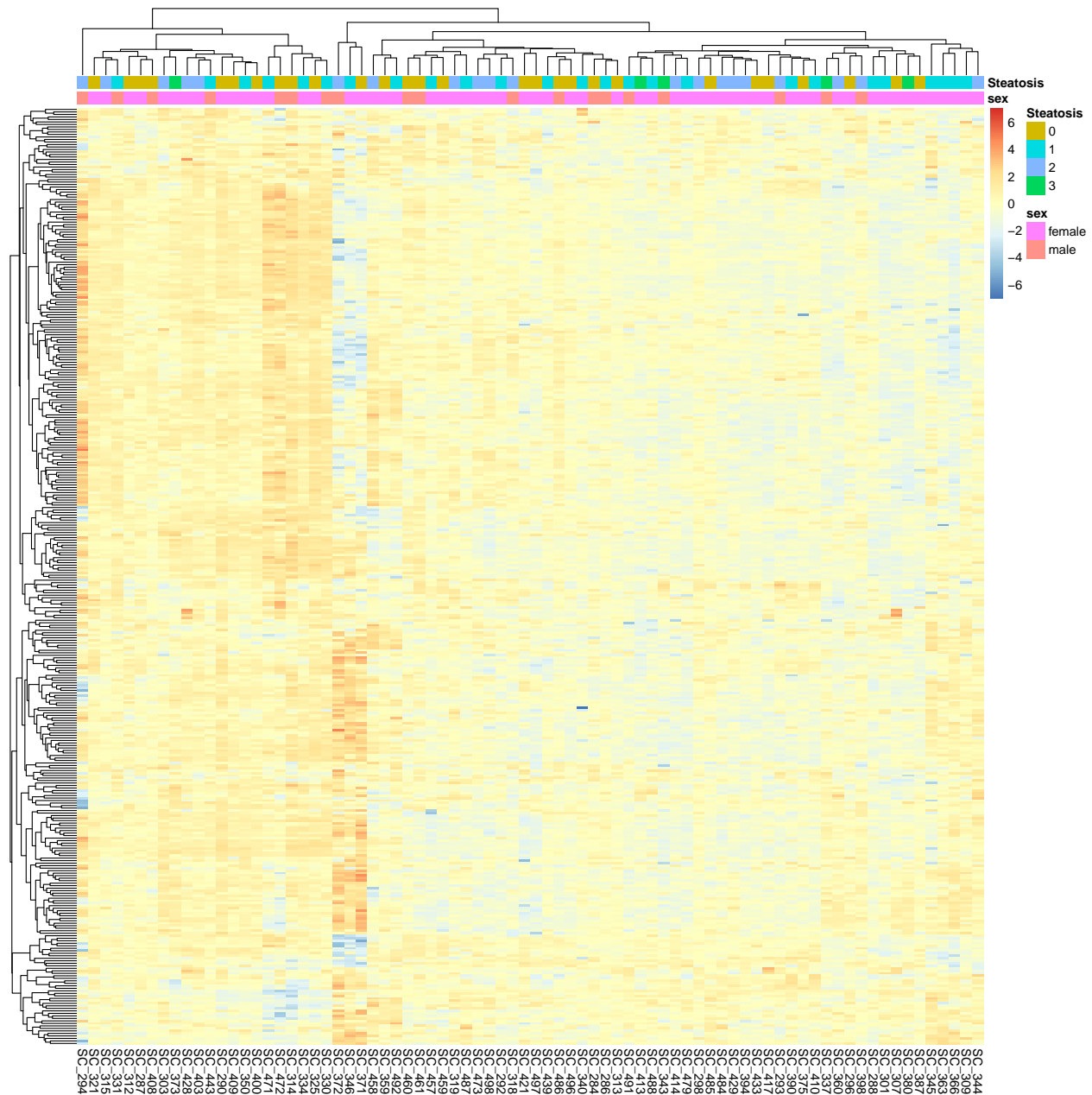
Figure 4.10: The heatmap illustrates the expression of 374 individual miRNA sequences across the analyzed samples. In this visualization, shades of red indicate increased miRNA expression, whereas shades of blue denote reduced or absent miRNA expression. Although a substantial number of miRNAs were identified, no distinct grouping patterns emerged among the analyzed samples, suggesting heterogeneity in miRNA expression profiles across the dataset.

Following their identification, we further analyzed the expression patterns of these two differentially expressed miRNAs by representing their normalized counts in boxplots across the four steatosis groups Figure 4.11.The boxplots highlight the consistency of expression changes across groups, reinforcing the relevance of these miRNAs in the context of steatosis severity. The miRNA *hsa-miR-144-3p* pattern of expression a significant decrease in expression as steatosis levels increase, whereas *hsa-miR-372-3p* exhibits a trend of progressively higher expression across the varying levels of steatosis.

Despite observing a trend of increasing expression of *hsa-miR-372-3p* with rising levels of steatosis, the results from the Kruskal-Wallis test did not achieve statistical significance ($p= 0.28$) when comparing the different states of steatosis. This suggests that, while there may be a tendency towards increased expression of the miRNA with the progression of steatosis, a larger sample size or an alternative approach is needed to draw firmer conclusions about its role in the progression of the disease.
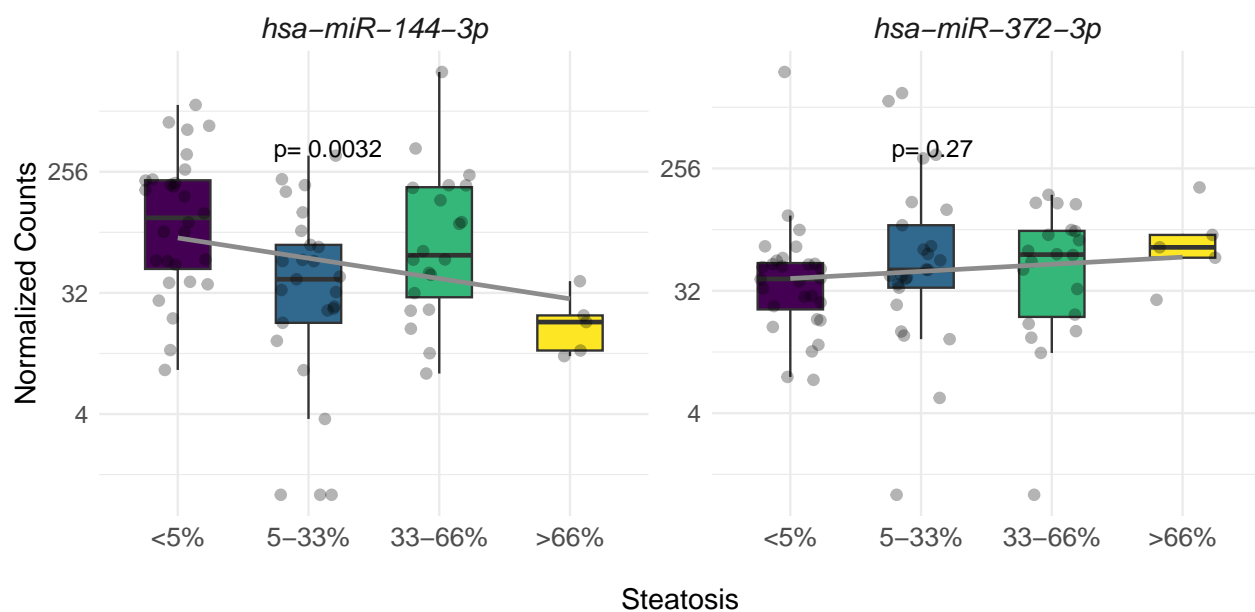
Figure 4.11: Boxplots of the differentially expressed miRNAs in subcutaneous white adipose tissue (scWAT) according to the four groups of steatosis. Each box represents the interquartile range (IQR) of the normalized counts, with the line inside the box indicating the median. The whiskers extend to show the range of the data, excluding outliers, which are displayed as individual points. *p*: p-value fot the Kruskal–Wallis test for the comparison between groups.

4.7 Target mRNA Selection and Validation

4.7.1 *hsa-miR-372-3p*

Potential target genes of the selected miRNAs were identified using the *multiMiR* package. This analysis included only validated interaction data, ensuring the biological relevance of the identified mRNAs. A subsequent filtering process was applied to select targets based on the type of experimental validation (e.g., luciferase assays, Western blot, or qRT-PCR) and functional support. As shown in Table 4.5, 24 target genes were identified after filtering.

Table 4.5: Selected interactions after filtering by database, experiment type (including luciferase assays, Western blot, or qRT-PCR), functional support (Functional MTI) and validated type for *hsa-miR-372-3p*.

Gene	Ensembl Identifier
LATS2	ENSG00000150457
TGFBR2	ENSG00000163513
NFIB	ENSG00000147862
CDKN1A	ENSG00000124762
VEGFA	ENSG00000112715
TNFAIP1	ENSG00000109079
TRPS1	ENSG00000104447
MBNL2	ENSG00000139793
RHOC	ENSG00000155366
NR4A2	ENSG00000153234
ERBB4	ENSG00000178568
CDK2	ENSG00000123374
LEFTY1	ENSG00000243709
BTG1	ENSG00000133639
WEE1	ENSG00000166483
CCNA1	ENSG00000133101
DKK1	ENSG00000107984
PHLPP2	ENSG00000040199
ATAD2	ENSG00000156802
ADAMTS9	ENSG00000163638
CADM2	ENSG00000175161
ZBTB7A	ENSG00000178951
TXNIP	ENSG00000265972
KLF13	ENSG00000275746

The target genes identified through *multiMiR* were subjected to functional enrichment analysis using KEGG (Kyoto Encyclopedia of Genes and Genomes) pathways[144]. The KEGG pathway enrichment analysis identified five significantly enriched pathways ($p < 0.05$) (Figure 4.12). The most prominent pathways include:

- *Cellular senescence* (KEGG ID: hsa04218): associated with cellular aging and the permanent arrest of the cell cycle in response to genetic damage, oxidative stress, or oncogenic signals.
- *Cell cycle* (KEGG ID: hsa04110): involved in the regulation and progression of the cell cycle, including critical checkpoints that ensure the fidelity of cell division.
- *Hepatitis B* (KEGG ID: hsa05161): related to infection by the hepatitis B virus and the inflammatory and carcinogenic processes it can trigger in the liver.
- *PI3K-Akt signaling pathway* (KEGG ID: hsa04151): a key pathway regulating cellular processes such as proliferation, survival, and metabolism, frequently deregulated in cancer. This pathway is related with insuline resistence.
- *Pancreatic cancer* (KEGG ID: hsa05212): associated with molecular and cellular alterations characteristic of this cancer type, including aberrant signaling and apoptosis resistance.

These pathways are primarily linked to essential processes such as *cell cycle regulation*, *intracellular signaling in cancer*, and *cellular responses to damage and infection*.
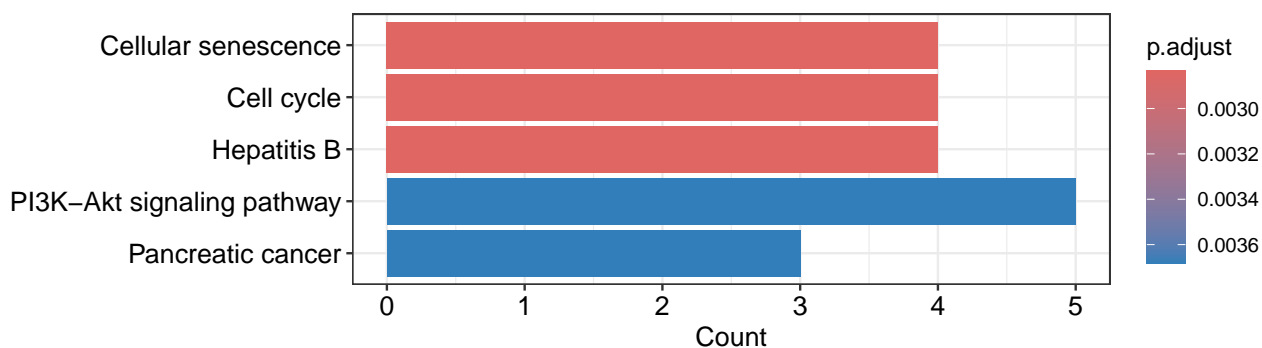
Figure 4.12: Top 5 Significant KEGG Pathways of *hsa-miR-372-3p*

4.7.2 *hsa-miR-144-3p*

Table 4.6 shows 22 target genes were identified for *hsa-miR-372-3p*, filtered by validated interactions and experimental evidence.

Table 4.6: Selected interactions after filtering by database, experiment type (including luciferase assays, Western blot, or qRT-PCR), functional support (Functional MTI) and validated type for *hsa-miR-144-3p*.

Gene	Ensembl Identifier
NOTCH1	ENSG00000148400
PLAG1	ENSG00000181690
ZEB1	ENSG00000148516
ZEB2	ENSG00000169554
IRS1	ENSG00000169047
MAP3K8	ENSG00000107968
EZH2	ENSG00000106462
APP	ENSG00000142192
PTGS2	ENSG00000073756
MET	ENSG00000105976
ETS1	ENSG00000134954
TGFB1	ENSG00000105329
CFTR	ENSG00000001626
FGG	ENSG00000171557
MTOR	ENSG00000198793
SMAD4	ENSG00000141646
NFE2L2	ENSG00000116044
PBX3	ENSG00000167081
TTN	ENSG00000155657
TUG1	ENSG00000253352
PTEN	ENSG00000284792

XIST   ENSG00000229807

The target genes identified through *multiMiR* were subjected to functional enrichment analysis using KEGG where five significantly enriched pathways ($p < 0.05$) (Figure 4.13). The most prominent pathways include:

- *MicroRNAs in cancer* (KEGG ID: hsa05206): Highlighting the role of miRNAs in the regulation of gene expression, particularly in pathways associated with tumorigenesis and cancer progression.

- *Hepatocellular carcinoma* (KEGG ID: hsa05225): Specifically linked to liver cancer and the molecular mechanisms underlying its development and progression.

- *FoxO signaling pathway* (KEGG ID: hsa04068): A critical pathway regulating oxidative stress response, apoptosis, and metabolism, which plays a significant role in cancer and aging.

- *Gastric cancer* (KEGG ID: hsa05226): Associated with molecular and cellular alterations characteristic of gastric tumorigenesis.

- *Cellular senescence* (KEGG ID: hsa04218): Related to aging and the permanent arrest of the cell cycle due to stress signals or damage.
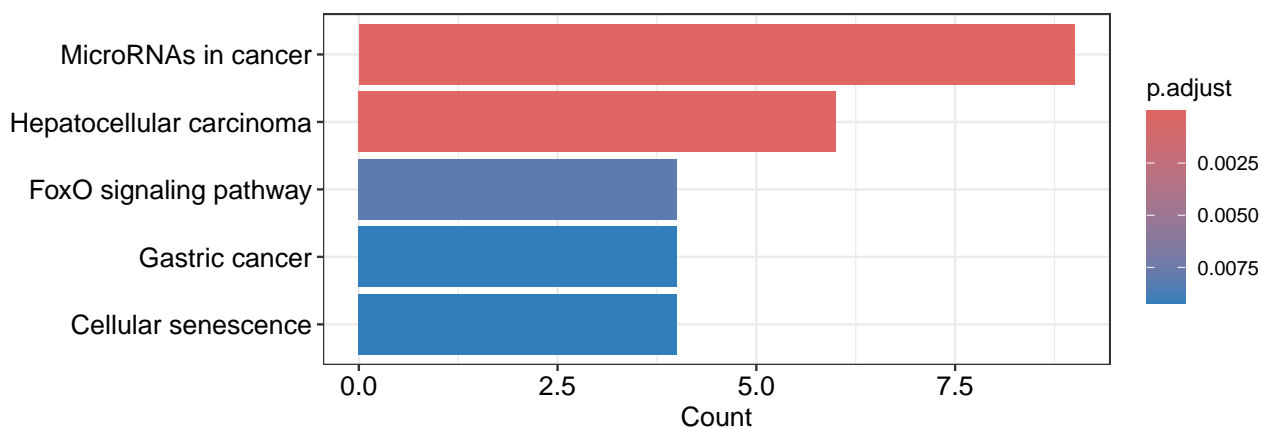
Figure 4.13: Top 5 Significant KEGG Pathways of *hsa-miR-144-3p*

These pathways reflect key biological processes, including tumorigenesis, stress response, and cell cycle regulation, underscoring the importance of miRNAs in these mechanisms. The findings provide valuable insights into potential molecular interactions and pathways relevant to the studied system.

4.8   The *hsa-miR-372-3p* and *hsa-miR-144-3p* in an in vitro model of lipid steatosis.

The gene expression was evaluated in HepG2 cells transfected for 24 hours and then treated with Oleic Acid (OA) for an additional 24 hours to assess the impact of single miRNA in a

cell model mimicking hepatic steatosis. Specifically, we investigated the relative expression of *PPARG* (Peroxisome Proliferator Activated Receptor Gamma), a key regulator of adipogenesis and insulin sensitivity; *PNPLA2* (Patatin Like Phospholipase Domain Containing 2), which encodes the Adipose Triglyceride Lipase (*ATGL*) involved in triglyceride breakdown; *DGAT2* (Diacylglycerol O-Acyltransferase 2), a critical enzyme for triglyceride synthesis; *FAS* (Fas Cell Surface Death Receptor), a mediator of apoptosis and cellular stress; and *ACACA* (Acetyl-CoA Carboxylase Alpha), the rate-limiting enzyme in *de novo* fatty acid synthesis. These genes play pivotal roles in lipid metabolism and, to a lesser extent, glucose metabolism, making them relevant targets for understanding the molecular mechanisms underlying hepatic steatosis.

The synthetic *miR-372* mimic significantly downregulated the mRNA expression of the gene *ACAC* (-91.40% ± 3.39; $p < 0.05$) in OA-treated HepG2 cells. A similar, although not statistically significant, decrease was observed in the mRNA levels of *FAS* (-90.50% ± 4.30; $p < 0.093$), suggesting a trend towards reduced expression. In contrast, the mRNA levels of *DGAT2* (-73.7% ± 6.70; $p = 0.462$) and *PNPLA2* (-55.10% ± 19.56; $p = 0.243$) did not show significant changes. Notably, the mRNA levels of *PPARG* remained unchanged compared to the negative control cells (Figure 4.14).
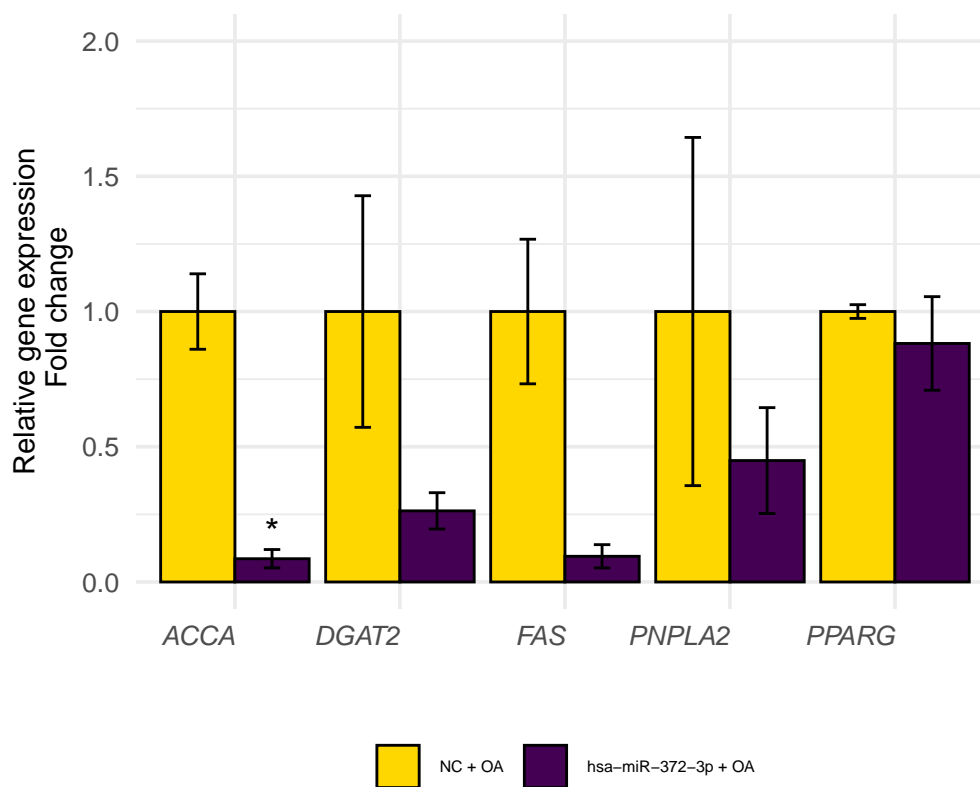
Description: The mRNA levels of protein–coding genes *ACCA, DGAT2, FAS, PNPLA2,PPARG*, involved in glucose and lipid metabolism, were assessed. HepG2 cells were transfected with 50 nM of mirVana mimic *miR–372–3p* (5'–AAAGUGCUGCGACAUUUGAGCGU–3') along with a randomized sequence as control (Negative Control 1). Twenty–four hours post–transfection, cells were treated with oleic acid (0.5 mM) for 24 hours. Results are mean relative gene expression ± SEM (n = 3).
Abbreviations: *NC* (negative control), *OA* (Oleic Acid), *ACCA* (Acetyl–CoA Carboxylase Alpha), *DGAT2* (Diacylglycerol O–Acyltransferase 2), *FAS* (Fatty Acid Synthase), *PNPLA2* (Patatin–like phospholipase domain–containing protein 2), *PPARG* (Peroxisome Proliferator Activated Receptor Gamma). *p*–value: * $p < 0.05$.

Figure 4.14: Gene expression analysis of HepG2 cells transfected with *miR-372-3p* mimic and negative control (scramble sequence) were treated with oleic acid to mimic in vitro hepatic steatosis.

On the other hand, inhibition of *hsa-miR-144-3p* upregulated the expression of the genes involved in lipid metabolism.. The relative gene expression levels of the evaluated targets in HepG2 cells transfected and treated with Oleic Acid (OA) were as follows: *ACACA* (96.80% ± 53.79; p = 0.186), *FAS* (135% ± 160.34; p = 0.429), *DGAT2* (32.74% ± 24.13; p = 0.128), *PNPLA2* (48.83% ± 14.32; p = 0.140), and *PPARG* (64.09% ± 41.25; p = 0.239) (Figure 4.14). Although the expression levels varied across genes, none of these changes were statistically significant ($p > 0.05$). These findings suggest that the regulatory effect of *hsa-miR-144-3p* on these genes may be limited under the experimental conditions employed.
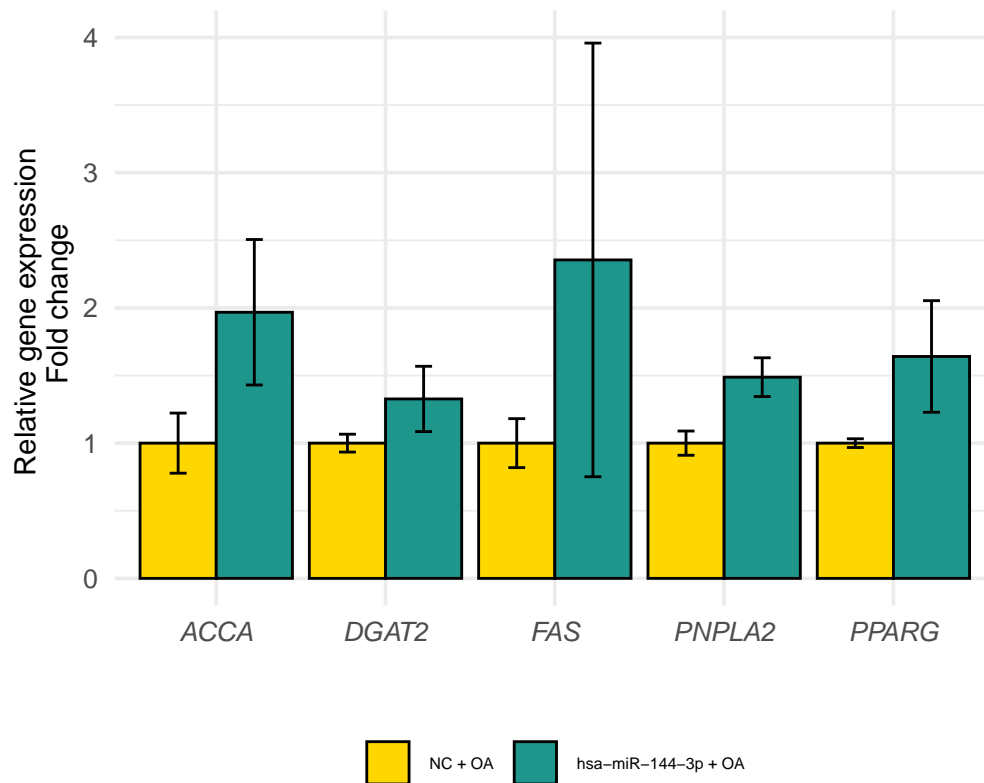
Description: The mRNA levels of protein–coding genes *ACCA, DGAT2, FAS, PNPLA2,PPARG*, involved in glucose and lipid metabolism, were assessed. HepG2 cells were transfected with 50 nM of mirVana mimic *mmiR–144–3p* (5'–UACAGUAUAGAUGAUGUACU–3') along with a randomized sequence as control (Negative Control 1). Twenty–four hours post–transfection, cells were treated with oleic acid (0.5 mM) for 24 hours. Results are mean relative gene expression ± SEM (n = 3).
Abbreviations: *NC* (negative control), *OA* (Oleic Acid), *ACCA* (Acetyl–CoA Carboxylase Alpha), *DGAT2* (Diacylglycerol O–Acyltransferase 2), *FAS* (Fatty Acid Synthase), *PNPLA2* (Patatin–like phospholipase domain–containing protein 2), *PPARG* (Peroxisome Proliferator Activated Receptor Gamma). *p*–value: * $p < 0.05$.

Figure 4.15: Gene expression analysis of HepG2 cells transfected with *miR-144-3p* inhibitor and negative control (scramble sequence) were treated with oleic acid to mimic in vitro hepatic steatosis.

Chapter 5

Discussion

This study presents new insights about the role of miRNAs from subcutaneous adipose tissue in regulating metabolic processes related to hepatic steatosis. Through the analysis of smRNA-seq, differential miRNAs linked to key metabolic pathways were identified that may play a role in liver fat accumulation and the progression of hepatic steatosis in obese individuals. These findings address a critical gap in understanding the role of miRNAs in adipose-liver metabolic crosstalk, which has implications for targeted interventions in hepatic steatosis and bring new avenues for their eventual use as biomakers.

Previous studies have extensively investigated the role of miRNAs as potential biomarkers in MASLD and HCC, highlighting their regulatory functions in disease development and progression at various levels[119,149–152]. Among these, *miRNA-34a* and *miRNA-122* stand out as the most extensively studied in MASLD patients[153,154]. Furthermore, other miRNAs have also been associated with MASLD, as shown in studies by Liu et al., Gjorgjieva et al., and Szabo et al.[73,153,155]. Notably, *miR-122-5p*, *miR-151a-3p*, *miR-126-5p*, and *miR-21-5p* have been proposed as predictive biomarkers for assessing MASLD at different stages of dietary interventions[156,157].

Beyond MASLD, miRNAs have been widely associated with other metabolic dysfunction-related disorders, including diabetes and T2DM[72]. For instance, tissue and circulating miRNAs have been identified as biomarkers of response to obesity treatment strategies in diseases such as diabetes[158].

Lastly, specific miRNAs have also been proposed as biomarkers in liver steatosis. Early studies identified miRNAs promising indicators of liver dysfunction[159], while others analyzed their expression in human omental and subcutaneous adipose tissue[152]. These findings emphasize the relevance of miRNAs not only in MASLD but also in broader contexts of metabolic and hepatic diseases.

In contrast to these previous studies, to our knowledge, our study is the first to identify differentially expressed miRNAs in subcutaneous with sm-RNA seq in scWAT from 78 obese individuals within the FATe cohort, which encompasses different scales of hepatic steatosis, and being validated *in vitro* through a model of human hepatocyte cells. Building on these insights, we specifically focused on identifying differentially expressed miRNAs associated with hepatic steatosis in subcutaneous adipose tissue to understand the direct relationship between hepatic steatosis and the expression of specific miRNAs in subcutaneous adipose tissue.

Understanding the expression patterns of miRNAs across different tissues is essential for gaining

deeper insights into both normal development and disease progression in these tissues[160]. Adipose tissue–liver crosstalk has been proposed to occur during MASLD, with factors originating from both adipose tissue and the liver identified as potential drivers of disease progression. Among these factors, miRNAs stand out, as their dysregulation in metabolic disturbances suggests a direct involvement in such conditions[161]. This highlights that alterations in miRNA signaling may play a role in obesity, metabolic syndrome, or MASLD.

hsa-miR-372-3p has been identified as a potent miRNA associated with tumorigenesis[162]. It has been shown to promote tumor formation in testicular germ cell tumors[163,164], lung cancer[165], parathyroid carcinoma[162], and osteosarcoma[166]. However, recent studies have highlighted the role of *hsa-miR-372-3p* in the context of MASH. Specifically, metabolic dysregulation leads to an increased expression of adipocyte enhancer binding protein 1 (*AEBP1*) in liver cells[167]. Its emerging role in the formation of collagen-rich tissues and the development of tissue fibrosis is also significant in the context of MASH[168]. Also, *AEBP1* is a key component of a group of genes specifically dysregulated in the fibrotic processes associated with MASH[72]. Notably, the levels of *hsa-miR-372-3p* is found to be lower in patients with MASH and advanced fibrosis, where this miRNA interact functionally with *AEBP1* to reduce its expression. This suggests that the dysregulation of this miRNA may contribute to the progression of hepatic steatosis and its associated complications, further linking *hsa-miR-372-3p* to the metabolic dysregulation observed in MASH[168].

Through transcriptomic and pathway analysis, we predicted additional pathways already experimentally validated in which *hsa-miR-372-3p* is implicated. These pathways support its role in tumorigenesis, they also suggest a broader implication of *hsa-miR-372-3p* in metabolic disorders, particularly in processes associated with liver fat accumulation and fibrosis progression. One of these predicted pathways is the *PI3K-Akt signaling pathway*, which plays a central role in regulating cell survival, metabolism, and inflammation. Dysregulation of this pathway has been linked to MASLD, particularly in the context of insulin resistance and abnormalities in lipid metabolism[169,170]. Moreover, its downregulation in patients with advanced fibrosis suggests a potential regulatory role in the progression of hepatic steatosis to more severe conditions such as MASLD and hepatocellular carcinoma (HCC)[162,168,171]. This highlight a dual role for *hsa-miR-372-3p* in tumorigenesis and metabolic regulation.

In this study, *hsa-mir-372-3p* was identified to be over-expressed in scWAT of obese patients with hepatic steatosis. However, it was significantly downregulated in MASH patients with advanced fibrosis compared to those with normal liver histology[168]. This change in expression underscores the potential role of *hsa-miR-372-3p* in the transition from simple steatosis to more severe liver conditions.

In our *in vitro* studies using HepG2 cells, the mimic of *hsa-miR-372-3p* downregulated the expression of *ACCA*, a key gene involved in lipogenesis. This finding aligns with the observed trends towards reduced mRNA levels of *FAS* and indicates a potential regulatory role of *hsa-miR-372-3p* in lipid metabolism. Although genes such as *DGAT2* and *PNPLA2* showed downregulation trends, they did not reach statistical significance, nor did *PPARG*, which remained unchanged.

These results suggest that *hsa-miR-372-3p* may influence hepatic lipid metabolism and contribute to the progression of hepatic steatosis, indicating its potential relevance in MASH pathogenesis. Although the result does not align with what might have been expected, the observed downregulation of key lipogenic genes, such as *ACCA* and *FAS*, reinforces the hypothesis that alterations in miRNA expression can significantly impact metabolic processes in the liver. *ACCA* is essential

for converting acetyl-CoA into malonyl-CoA, a critical step in fatty acid synthesis, while FAS is responsible for synthesizing long-chain fatty acids.

Interestingly, the downregulation of *ACACA* and *FAS* observed in our study could be partially mediated by the *PI3K-Akt pathway*, as this signaling cascade is closely tied to lipogenesis and lipid metabolism. This suggests a possible interaction between *hsa-miR-372-3p* and key metabolic signaling pathways, further underscoring its central role in hepatic lipid regulation.

hsa-miR-372-3p has been proposed as a regulatory miRNA in MASH[172], and the observed down-regulation of critical lipogenic genes highlights the need for further investigation into the functional implications of this miRNA and its targets in the context of liver disease. These findings also open avenues for therapeutic strategies targeting *hsa-miR-372-3p*, potentially providing a novel approach to managing lipid accumulation and fibrosis in MASLD.

hsa-mir-144-3p belongs to the *MIR-144* family, alongside its counterpart, the guide strand *hsa-mir-144-5p*. Although *hsa-mir-144-3p* is technically classified as the passenger strand, studies have demonstrated that it is often more abundant than the guide strand and plays a significant functional role in the organism[173]. This highlights the need to consider both strands when analyzing the biological impact of the *MIR-144* family. This miRNAs is typically secreted into the extracellular space[174] and is frequently expressed in liver pathology[175]. Furthermore, *MIR-144* has been implicated in the progression of various cancers[176]. In the context of liver-related metabolic diseases, these miRNAs have been associated with pathologies such as chronic hepatitis B and HCC[175,177].

In our analyses, *hsa-miR-144-3p* emerged as a differentially expressed miRNA, suggesting its relevance in the context of hepatic steatosis. Previous studies have reported that this miRNA is involved in the progression of insulin resistance, which is closely linked to the development of hepatic steatosis and other metabolic disorders[72]. Additionally, *hsa-miR-144-3p* has been shown to inhibit nuclear factor erythroid 2-related factor 2 (*Nrf2*) expression and downstream antioxidant genes, which in turn reduces glucose consumption and exacerbates zinc-induced insulin resistance in HepG2 cells[178].

Furthermore, previous studies found that the upregulation of *hsa-miR-144-3p* promotes hepatocyte proliferation by suppressing the expression of the *Txnip* gene (thioredoxin-interacting protein), which is involved in glucose metabolism and inhibition of cell proliferation. This suggests that this miRNA could play a crucial role in liver regeneration, making it a promising therapeutic target for hepatic steatosis and related conditions[179]. These findings indicate that *hsa-miR-144-3p* is involved in liver regeneration and gluconeogenesis, making it an interesting candidate for investigating its role in hepatic steatosis. Indeed, several studies have already described a causative role of this miRNA in liver steatosis/liver disease ([100];[180];[177]).

Through transcriptomic and pathway analysis, we predicted additional pathways that have been experimentally validated in which *hsa-miR-144-3p* is implicated. Among these pathways, the *FoxO signaling pathway* has been established as a fundamental regulator in hepatic metabolism for its interaction with CCAAT/enhancer-binding protein alpha (*C/EBPα*), a crucial regulator of adipogenesis. This highlights its relevance in metabolic homeostasis and preadipocyte differentiation and also related[181]. Indeed, this pathway have been associated with MASLD[182].

Moreover, *hsa-miR-144-3p* is downregulated in patients with HCC[177]. Studies have reported that the suppression of this miRNA promotes proliferation and metastasis by targeting E2F transcription factor 3 (*E2F3*), an oncogene involved in the regulation of cell proliferation[176,183]. In our study,

we found that the expression of *hsa-miR-144-3p* significantly decreases as the level of steatosis increases in scWAT, suggesting a potential link between this miRNA's regulatory function and the progression of hepatic metabolic disorders. These findings underscore the importance of *hsa-miR-144-3p* as a candidate for therapeutic targeting in HCC and related metabolic conditions.

Furthermore, inhibition of *hsa-miR-144-3p* led to an upregulation of its key genes involved in the regulation of lipid metabolism in HepG2 cells treated with oleic acid. While the expression levels of the evaluated targets displayed variations, the changes did not reach statistical significance, indicating that the influence of *hsa-miR-144-3p* on these genes might be constrained under the experimental conditions utilized. This suggests that, despite the potential regulatory role of hsa-miR-144-3p, the specific context and cellular environment can significantly impact its effectiveness in modulating gene expression.

The potential of *hsa-miR-144-3p* extends beyond its role in liver metabolism and cancer progression. It has been proposed as a promising therapeutic target and a diagnostic/prognostic tool in various cancers[176,184]. Specifically, Rowe et al.[175] suggest that hsa-miR-144 could serve as a valuable biomarker in blood, plasma, or serum for chronic hepatitis B. This highlights the versatility of *hsa-miR-144-3p* not only in understanding disease mechanisms but also in facilitating early diagnosis and targeted therapies, reinforcing its importance in both clinical and research settings.

One of the main strengths of this study lies in the use of smRNA-seq analysis to identify specific miRNAs scWAT, an innovative methodology that provides detailed and accurate information about their regulation compared to previous studies. Furthermore, this is the first study to differentially characterize miRNAs in a large cohort of 78 patients with obesity. The identification of *hsa-miR-372-3p* and *hsa-miR-144-3p* as key regulators in metabolic pathways related to lipogenesis and the progression of hepatic steatosis, along with their functional validation in *in vitro* models, reinforces the biological and clinical relevance of the findings. This approach also provides new insights into the metabolic interaction between scWAT and the liver, highlighting the potential of these miRNAs as biomarkers and therapeutic targets in the management of obesity and its hepatic complications.

Despite these strengths, the study has several limitations. First, a greater representation of the later stages of steatossi progression would strengthen the findings, as although the number of volunteers is significant, the number of severe cases is relatively low. Nevertheless, a sample of 80 individuals is robust and provides solid statistical power. Second, while HepG2 cells served as a convenient model for our in vitro studies, their limitations in fully mimicking adipose-liver cross-talk restrict the scope of our findings. An adipocyte model could have provided a more physiologically relevant system for studying the interplay between *hsa-miR-144-3p* and *hsa-miR-372-3p* and metabolic pathways. However, due to time constraints, this alternative was not feasible within the framework of this study. Future research should address these limitations by incorporating diverse cellular models and larger datasets to strengthen the generalizability and applicability of our conclusions.

This study highlights the role of miRNAs expressed in adipose tissue in the regulation of metabolic processes related to hepatic steatosis. We identified *hsa-miR-372-3p* and *hsa-miR-144-3p* as key regulators in metabolic pathways such as lipogenesis and confirmed their functional impact *in vitro* models of hepatocytes. These findings reinforce their potential as biomarkers and therapeutic targets for the management of obesity and its hepatic complications.

Chapter 6

Conclusions

1. MiRNAs derived from subcutaneous adipose tissue play a fundamental role in regulating metabolic processes related to hepatic steatosis, suggesting that their expression may influence the progression of liver diseases.

2. Specific miRNAs, such as *hsa-miR-372-3p* and *hsa-miR-144-3p*, have been identified as potential biomarkers for the diagnosis and prognosis of hepatic steatosis and its complications, opening new opportunities for personalized medicine.

3. This study enhances the understanding of the relationship between adipose tissue and the liver, highlighting how miRNAs may be involved in regulating lipid accumulation and disease progression.

4. Further investigations are needed to validate these findings and explore the therapeutic potential of miRNAs in treating hepatic steatosis and other metabolic disorders.

5. The results of this study contribute to the current understanding of metabolic health, suggesting that modulation of miRNAs may offer novel strategies to address health issues related to obesity and liver diseases.

References

1. Angulo, P. (2007). Obesity and nonalcoholic fatty liver disease. *Nutrition Reviews*, *65*(suppl_1), S57–S63.
2. Idilman, I. S., Ozdeniz, I., & Karcaaltincaba, M. (2016). Hepatic steatosis: Etiology, patterns, and quantification. *Seminars in Ultrasound, CT and MRI*, *37*, 501–510.
3. Brankovic, M., Jovanovic, I., Dukic, M., Radonjic, T., Opric, S., Klavsnja, S., & Zdravkovic, M. (2022). Lipotoxity as the leading cause of non-alcoholic steatohepatitis. *International Journal of Molecular Sciences*, *23*(9), 5146.
4. Mary, E., Jeffrey, V., Ratziu, V., Sven, M., Arun, J., Kanwal, F., Romero, D., Manal, F., Quentin, M., Arab, J. P., et al. (2024). A multisociety delphi consensus statement on new fatty liver disease nomenclature. *Annals of Hepatology*, *29*(1), 1–15.
5. Wong, R. J. (2024). Epidemiology of metabolic dysfunction-associated steatotic liver disease (MASLD) and alcohol-related liver disease (ALD). *Metabolism and Target Organ Damage*, *4*(4), N–A.
6. Thyfault, J. P., & Rector, R. S. (2020). Exercise combats hepatic steatosis: Potential mechanisms and clinical implications. *Diabetes*, *69*(4), 517–524.
7. Chan, W.-K., Chuah, K.-H., Rajaram, R. B., Lim, L.-L., Ratnasingam, J., & Vethakkan, S. R. (2023). Metabolic dysfunction-associated steatotic liver disease (MASLD): A state-of-the-art review. *Journal of Obesity & Metabolic Syndrome*, *32*(3), 197.
8. Younossi, Z. M. (2019). Non-alcoholic fatty liver disease–a global public health perspective. *Journal of Hepatology*, *70*(3), 531–544.
9. Ma, Y., Wang, J., Xiao, W., & Fan, X. (2024). A review of MASLD-related hepatocellular carcinoma: Progress in pathogenesis, early detection, and therapeutic interventions. *Frontiers in Medicine*, *11*, 1410668.
10. Sarwar, R., Pierce, N., & Koppe, S. (2018). Obesity and nonalcoholic fatty liver disease: Current perspectives. *Diabetes, Metabolic Syndrome and Obesity: Targets and Therapy*, 533–542.
11. Miao, L., Targher, G., Byrne, C. D., Cao, Y.-Y., & Zheng, M.-H. (2024). Current status and future trends of the global burden of MASLD. *Trends in Endocrinology & Metabolism*.
12. Younossi, Z. M., Koenig, A. B., Abdelatif, D., Fazel, Y., Henry, L., & Wymer, M. (2016). Global epidemiology of nonalcoholic fatty liver disease—meta-analytic assessment of prevalence, incidence, and outcomes. *Hepatology*, *64*(1), 73–84.
13. Younossi, Z. M., Golabi, P., Avila, L. de, Paik, J. M., Srishord, M., Fukui, N., Qiu, Y., Burns, L., Afendy, A., & Nader, F. (2019). The global epidemiology of NAFLD and NASH in patients with type 2 diabetes: A systematic review and meta-analysis. *Journal of Hepatology*, *71*(4), 793–801.
14. Paik, J. M., Henry, L., Younossi, Y., Ong, J., Alqahtani, S., & Younossi, Z. M. (2023). The burden of nonalcoholic fatty liver disease (NAFLD) is rapidly growing in every region of the world from 1990 to 2019. *Hepatology Communications*, *7*(10), e0251.
15. Younossi, Z. M., Golabi, P., Paik, J. M., Henry, A., Van Dongen, C., & Henry, L. (2023). The global

epidemiology of nonalcoholic fatty liver disease (NAFLD) and nonalcoholic steatohepatitis (NASH): A systematic review. *Hepatology*, *77*(4), 1335–1347.

16. Younossi, Z., Anstee, Q. M., Marietti, M., Hardy, T., Henry, L., Eslam, M., George, J., & Bugianesi, E. (2018). Global burden of NAFLD and NASH: Trends, predictions, risk factors and prevention. *Nature Reviews Gastroenterology & Hepatology*, *15*(1), 11–20.

17. Caballería, L., Pera, G., Auladell, M. A., Torán, P., Muñoz, L., Miranda, D., Alumá, A., Casas, J. D., Sánchez, C., Gil, D., et al. (2010). Prevalence and factors associated with the presence of nonalcoholic fatty liver disease in an adult population in spain. *European Journal of Gastroenterology & Hepatology*, *22*(1), 24–32.

18. Kershaw, E. E., & Flier, J. S. (2004). Adipose tissue as an endocrine organ. *The Journal of Clinical Endocrinology & Metabolism*, *89*(6), 2548–2556.

19. Rosen, E. D., & Spiegelman, B. M. (2014). What we talk about when we talk about fat. *Cell*, *156*(1), 20–44.

20. Cinti, S. (2007). The adipose organ. *Adipose Tissue and Adipokines in Health and Disease*, 3–19.

21. Zwick, R. K., Guerrero-Juarez, C. F., Horsley, V., & Plikus, M. V. (2018). Anatomical, physiological, and functional diversity of adipose tissue. *Cell Metabolism*, *27*(1), 68–83.

22. Cinti, S. (2019). Anatomy and physiology of the nutritional system. *Molecular Aspects of Medicine*, *68*, 101–107.

23. Lopez-Yus, M., Hörndler, C., Borlan, S., Bernal-Monterde, V., & Arbones-Mainar, J. M. (2024). Unraveling adipose tissue dysfunction: Molecular mechanisms, novel biomarkers, and therapeutic targets for liver fat deposition. *Cells*, *13*(5), 380.

24. Ghesmati, Z., Rashid, M., Fayezi, S., Gieseler, F., Alizadeh, E., & Darabi, M. (2024). An update on the secretory functions of brown, white, and beige adipose tissue: Towards therapeutic applications. *Reviews in Endocrine and Metabolic Disorders*, *25*(2), 279–308.

25. Jialal, I., & Devaraj, S. (2018). Subcutaneous adipose tissue biology in metabolic syndrome. *Hormone Molecular Biology and Clinical Investigation*, *33*(1), 20170074.

26. Ibrahim, M. M. (2010). Subcutaneous and visceral adipose tissue: Structural and functional differences. *Obesity Reviews*, *11*(1), 11–18.

27. Kwok, K. H., Lam, K. S., & Xu, A. (2016). Heterogeneity of white adipose tissue: Molecular basis and clinical implications. *Experimental & Molecular Medicine*, *48*(3), e215–e215.

28. McQuaid, S. E., Humphreys, S. M., Hodson, L., Fielding, B. A., Karpe, F., & Frayn, K. N. (2010). Femoral adipose tissue may accumulate the fat that has been recycled as VLDL and nonesterified fatty acids. *Diabetes*, *59*(10), 2465–2473.

29. Koenen, M., Hill, M. A., Cohen, P., & Sowers, J. R. (2021). Obesity, adipose tissue and vascular dysfunction. *Circulation Research*, *128*(7), 951–968.

30. Scherer, P. E. (2006). Adipose tissue: From lipid storage compartment to endocrine organ. *Diabetes*, *55*(6), 1537–1545.

31. Song, Z., Xiaoli, A. M., & Yang, F. (2018). Regulation and metabolic significance of de novo lipogenesis in adipose tissues. *Nutrients*, *10*(10), 1383.

32. Carpentier, A. C. (2021). 100th anniversary of the discovery of insulin perspective: Insulin and adipose tissue fatty acid metabolism. *American Journal of Physiology-Endocrinology and Metabolism*, *320*(4), E653–E670.

33. Grabner, G. F., Xie, H., Schweiger, M., & Zechner, R. (2021). Lipolysis: Cellular mechanisms for lipid mobilization from fat stores. *Nature Metabolism*, *3*(11), 1445–1465.

34. Duncan, R. E., Ahmadian, M., Jaworski, K., Sarkadi-Nagy, E., & Sul, H. S. (2007). Regulation of lipolysis in adipocytes. *Annu. Rev. Nutr.*, *27*(1), 79–101.

35. Scheja, L., & Heeren, J. (2019). The endocrine function of adipose tissues in health and cardiometabolic disease. *Nature Reviews Endocrinology*, *15*(9), 507–524.

36. Friedman, J. (2019). *Leptin and the endocrine control of energy balance. Nat. Metab. 1*, *754–764.*

37. Karbowska, J., & Kochan, Z. (2006). Role of adiponectin in the regulation of carbohydrate and lipid metabolism. *Journal of Physiology and Pharmacology*, *57*, 103.

38. Bond, S. T., Calkin, A. C., & Drew, B. G. (2022). Adipose-derived extracellular vesicles: Systemic messengers and metabolic regulators in health and disease. *Frontiers in Physiology*, *13*, 837001.

39. Kulaj, K., Harger, A., Bauer, M., Caliskan, Ö. S., Gupta, T. K., Chiang, D. M., Milbank, E., Reber, J., Karlas, A., Kotzbeck, P., et al. (2023). Adipocyte-derived extracellular vesicles increase insulin secretion through transport of insulinotropic protein cargo. *Nature Communications*, *14*(1), 709.

40. Jung, U. J., & Choi, M.-S. (2014). Obesity and its metabolic complications: The role of adipokines and the relationship between obesity, inflammation, insulin resistance, dyslipidemia and nonalcoholic fatty liver disease. *International Journal of Molecular Sciences*, *15*(4), 6184–6223.

41. Zorena, K., Jachimowicz-Duda, O., Ślęzak, D., Robakowska, M., & Mrugacz, M. (2020). Adipokines and obesity. Potential link to metabolic disorders and chronic complications. *International Journal of Molecular Sciences*, *21*(10), 3570.

42. Jo, J., Gavrilova, O., Pack, S., Jou, W., Mullen, S., Sumner, A. E., Cushman, S. W., & Periwal, V. (2009). Hypertrophy and/or hyperplasia: Dynamics of adipose tissue growth. *PLoS Computational Biology*, *5*(3), e1000324.

43. Stenkula, K. G., & Erlanson-Albertsson, C. (2018). Adipose cell size: Importance in health and disease. *American Journal of Physiology-Regulatory, Integrative and Comparative Physiology*, *315*(2), R284–R295.

44. Muir, L. A., Neeley, C. K., Meyer, K. A., Baker, N. A., Brosius, A. M., Washabaugh, A. R., Varban, O. A., Finks, J. F., Zamarron, B. F., Flesher, C. G., et al. (2016). Adipose tissue fibrosis, hypertrophy, and hyperplasia: Correlations with diabetes in human obesity. *Obesity*, *24*(3), 597–605.

45. Trayhurn, P. (2013). Hypoxia and adipose tissue function and dysfunction in obesity. *Physiological Reviews*, *93*(1), 1–21.

46. Kawai, T., Autieri, M. V., & Scalia, R. (2021). Adipose tissue inflammation and metabolic dysfunction in obesity. *American Journal of Physiology-Cell Physiology*, *320*(3), C375–C391.

47. Wondmkun, Y. T. (2020). Obesity, insulin resistance, and type 2 diabetes: Associations and therapeutic implications. *Diabetes, Metabolic Syndrome and Obesity*, 3611–3616.

48. Ipsen, D. H., Lykkesfeldt, J., & Tveden-Nyborg, P. (2018). Molecular mechanisms of hepatic lipid accumulation in non-alcoholic fatty liver disease. *Cellular and Molecular Life Sciences*, *75*, 3313–3327.

49. Gray, S. L., & Vidal-Puig, A. J. (2007). Adipose tissue expandability in the maintenance of metabolic homeostasis. *Nutrition Reviews*, *65*(suppl_1), S7–S12.

50. Virtue, S., & Vidal-Puig, A. (2010). Adipose tissue expandability, lipotoxicity and the metabolic syndrome—an allostatic perspective. *Biochimica Et Biophysica Acta (BBA)-Molecular and Cell Biology of Lipids*, *1801*(3), 338–349.

51. Lee, E., Korf, H., & Vidal-Puig, A. (2023). An adipocentric perspective on the development and progression of non-alcoholic fatty liver disease. *Journal of Hepatology*, *78*(5), 1048–1062.

52. Du Plessis, J., Van Pelt, J., Korf, H., Mathieu, C., Van der Schueren, B., Lannoo, M., Oyen, T., Topal, B., Fetter, G., Nayler, S., et al. (2015). Association of adipose tissue inflammation with histologic severity of nonalcoholic fatty liver disease. *Gastroenterology*, *149*(3), 635–648.

53. Zhang, X.-Q., Xu, C.-F., Yu, C.-H., Chen, W.-X., & Li, Y.-M. (2014). Role of endoplasmic reticulum stress in the pathogenesis of nonalcoholic fatty liver disease. *World Journal of Gastroenterology: WJG*, *20*(7), 1768.

54. Wang, J., He, W., Tsai, P.-J., Chen, P.-H., Ye, M., Guo, J., & Su, Z. (2020). Mutual interaction

between endoplasmic reticulum and mitochondria in nonalcoholic fatty liver disease. *Lipids in Health and Disease*, *19*, 1–19.

55. Delli Bovi, A. P., Marciano, F., Mandato, C., Siano, M. A., Savoia, M., & Vajro, P. (2021). Oxidative stress in non-alcoholic fatty liver disease. An updated mini review. *Frontiers in Medicine*, *8*, 595371.

56. Paradies, G., Paradies, V., Ruggiero, F. M., & Petrosillo, G. (2014). Oxidative stress, cardiolipin and mitochondrial dysfunction in nonalcoholic fatty liver disease. *World Journal of Gastroenterology: WJG*, *20*(39), 14205.

57. Alkhouri, N., Dixon, L. J., & Feldstein, A. E. (2009). Lipotoxicity in nonalcoholic fatty liver disease: Not all lipids are created equal. *Expert Review of Gastroenterology & Hepatology*, *3*(4), 445–451.

58. Jacome-Sosa, M. M., & Parks, E. J. (2014). Fatty acid sources and their fluxes as they contribute to plasma triglyceride concentrations and fatty liver in humans. *Current Opinion in Lipidology*, *25*(3), 213–220.

59. Wronska, A., Kurkowska-Jastrzebska, I., & Santulli, G. (2015). Application of micro RNA s in diagnosis and treatment of cardiovascular disease. *Acta Physiologica*, *213*(1), 60–83.

60. Lauressergues, D., Couzigou, J.-M., Clemente, H. S., Martinez, Y., Dunand, C., Bécard, G., & Combier, J.-P. (2015). Primary transcripts of microRNAs encode regulatory peptides. *Nature*, *520*(7545), 90–93.

61. Van Rooij, E., & Olson, E. N. (2012). MicroRNA therapeutics for cardiovascular disease: Opportunities and obstacles. *Nature Reviews Drug Discovery*, *11*(11), 860–872.

62. Guo, H., Ingolia, N. T., Weissman, J. S., & Bartel, D. P. (2010). Mammalian microRNAs predominantly act to decrease target mRNA levels. *Nature*, *466*(7308), 835–840.

63. Lee, R. C., Feinbaum, R. L., & Ambros, V. (1993). The c. Elegans heterochronic gene lin-4 encodes small RNAs with antisense complementarity to lin-14. *Cell*, *75*(5), 843–854.

64. Wightman, B., Ha, I., & Ruvkun, G. (1993). Posttranscriptional regulation of the heterochronic gene lin-14 by lin-4 mediates temporal pattern formation in c. elegans. *Cell*, *75*(5), 855–862.

65. Calin, G. A., Hubé, F., Ladomery, M. R., Delihas, N., Ferracin, M., Poliseno, L., Agnelli, L., Alahari, S. K., Yu, A.-M., & Zhong, X.-B. (2024). The 2024 nobel prize in physiology or medicine: microRNA takes center stage. In *Non-Coding RNA* (6; Vol. 10, p. 62). MDPI.

66. Vienberg, S., Geiger, J., Madsen, S., & Dalgaard, L. T. (2017). Micro RNA s in metabolism. *Acta Physiologica*, *219*(2), 346–361.

67. Alles, J., Fehlmann, T., Fischer, U., Backes, C., Galata, V., Minet, M., Hart, M., Abu-Halima, M., Grässer, F. A., Lenhof, H.-P., et al. (2019). An estimate of the total number of true human miRNAs. *Nucleic Acids Research*, *47*(7), 3353–3364.

68. Catalanotto, C., Cogoni, C., & Zardo, G. (2016). MicroRNA in control of gene expression: An overview of nuclear functions. *International Journal of Molecular Sciences*, *17*(10), 1712.

69. Santulli, G. (2015). *MicroRNA: Basic science: From molecular biology to clinical practice* (Vol. 887). Springer.

70. Yates, L. A., Norbury, C. J., & Gilbert, R. J. (2013). The long and short of microRNA. *Cell*, *153*(3), 516–519.

71. Arrighetti, N., & Beretta, G. L. (2021). miRNAs as therapeutic tools and biomarkers for prostate cancer. *Pharmaceutics*, *13*(3), 380.

72. Ma, N., Tan, J., Chen, Y., Yang, L., Li, M., & He, Y. (2024). MicroRNAs in metabolic dysfunction-associated diseases: Pathogenesis and therapeutic opportunities. *The FASEB Journal*, *38*(17), e70038.

73. Gjorgjieva, M., Sobolewski, C., Dolicka, D., Sousa, M. C. de, & Foti, M. (2019). miRNAs and NAFLD: From pathophysiology to therapy. *Gut*, *68*(11), 2065–2079.

74. Liu, W., Cao, H., Yan, J., Huang, R., & Ying, H. (2015). Micro-managers of hepatic lipid metabolism and NAFLD. *Wiley Interdisciplinary Reviews: RNA*, *6*(5), 581–593.

75. Bartel, D. P. (2004). MicroRNAs: Genomics, biogenesis, mechanism, and function. *Cell*, *116*(2), 281–297.

76. Winter, J., Jung, S., Keller, S., Gregory, R. I., & Diederichs, S. (2009). Many roads to maturity: microRNA biogenesis pathways and their regulation. *Nature Cell Biology*, *11*(3), 228–234.

77. Denli, A. M., Tops, B. B., Plasterk, R. H., Ketting, R. F., & Hannon, G. J. (2004). Processing of primary microRNAs by the microprocessor complex. *Nature*, *432*(7014), 231–235.

78. Lee, Y., Kim, M., Han, J., Yeom, K.-H., Lee, S., Baek, S. H., & Kim, V. N. (2004). MicroRNA genes are transcribed by RNA polymerase II. *The EMBO Journal*, *23*(20), 4051–4060.

79. Zeng, Y., Yi, R., & Cullen, B. R. (2005). Recognition and cleavage of primary microRNA precursors by the nuclear processing enzyme drosha. *The EMBO Journal*, *24*(1), 138–148.

80. Shiohama, A., Sasaki, T., Noda, S., Minoshima, S., & Shimizu, N. (2003). Molecular cloning and expression analysis of a novel gene DGCR8 located in the DiGeorge syndrome chromosomal region. *Biochemical and Biophysical Research Communications*, *304*(1), 184–190.

81. Katahira, J., & Yoneda, Y. (2011). Nucleocytoplasmic transport of microRNAs and related small RNAs. *Traffic*, *12*(11), 1468–1474.

82. Bhayani, M. K., Calin, G. A., & Lai, S. Y. (2012). Functional relevance of miRNA* sequences in human disease. *Mutation Research/Fundamental and Molecular Mechanisms of Mutagenesis*, *731*(1-2), 14–19.

83. O'Brien, J., Hayder, H., Zayed, Y., & Peng, C. (2018). Overview of microRNA biogenesis, mechanisms of actions, and circulation. *Frontiers in Endocrinology*, *9*, 402.

84. Gebert, L. F., & MacRae, I. J. (2019). Regulation of microRNA function in animals. *Nature Reviews Molecular Cell Biology*, *20*(1), 21–37.

85. Neilsen, C. T., Goodall, G. J., & Bracken, C. P. (2012). IsomiRs–the overlooked repertoire in the dynamic microRNAome. *Trends in Genetics*, *28*(11), 544–549.

86. Wahid, F., Shehzad, A., Khan, T., & Kim, Y. Y. (2010). MicroRNAs: Synthesis, mechanism, function, and recent clinical trials. *Biochimica Et Biophysica Acta (BBA)-Molecular Cell Research*, *1803*(11), 1231–1243.

87. Lim, L. P., Lau, N. C., Garrett-Engele, P., Grimson, A., Schelter, J. M., Castle, J., Bartel, D. P., Linsley, P. S., & Johnson, J. M. (2005). Microarray analysis shows that some microRNAs downregulate large numbers of target mRNAs. *Nature*, *433*(7027), 769–773.

88. Lv, Y., Yin, K., Fu, Y., Zhang, D., Chen, W., & Tang, C. (2013). Posttranscriptional regulation of ATP-binding cassette transporter A1 in lipid metabolism. *DNA and Cell Biology*, *32*(7), 348–358.

89. Friedman, R. C., Farh, K. K.-H., Burge, C. B., & Bartel, D. P. (2009). Most mammalian mRNAs are conserved targets of microRNAs. *Genome Research*, *19*(1), 92–105.

90. Agarwal, V., Bell, G. W., Nam, J.-W., & Bartel, D. P. (2015). Predicting effective microRNA target sites in mammalian mRNAs. *Elife*, *4*, e05005.

91. Chen, L., Heikkinen, L., Wang, C., Yang, Y., Sun, H., & Wong, G. (2019). Trends in the development of miRNA bioinformatics tools. *Briefings in Bioinformatics*, *20*(5), 1836–1852.

92. Lee, Y. H., Jang, H.-J., Kim, S., Choi, S. S., Khim, K. W., Eom, H., Hyun, J., Shin, K. J., Chae, Y. C., Kim, H., et al. (2021). Hepatic MIR20B promotes nonalcoholic fatty liver disease by suppressing PPARA. *Elife*, *10*, e70472.

93. Wang, Y.-D., Wu, L.-L., Mai, Y.-N., Wang, K., Tang, Y., Wang, Q.-Y., Li, J.-Y., Jiang, L.-Y., Liao, Z.-Z., Hu, C., et al. (2023). miR-32-5p induces hepatic steatosis and hyperlipidemia by triggering de novo lipogenesis. *Metabolism*, *146*, 155660.

94. Wang, D.-R., Wang, B., Yang, M., Liu, Z., Sun, J., Wang, Y., Sun, H., & Xie, L.-J. (2020). Suppression of miR-30a-3p attenuates hepatic steatosis in non-alcoholic fatty liver disease.

Biochemical Genetics, *58*, 691–704.

95. Liu, X., Chen, S., & Zhang, L. (2020). Downregulated microRNA-130b-5p prevents lipid accumulation and insulin resistance in a murine model of nonalcoholic fatty liver disease. *American Journal of Physiology-Endocrinology and Metabolism*, *319*(1), E34–E42.

96. Zeng, N., Huang, R., Li, N., Jiang, H., Li, R., Wang, F., Chen, W., Xia, M., & Wang, Q. (2018). MiR-451a attenuates free fatty acids–mediated hepatocyte steatosis by targeting the thyroid hormone responsive spot 14 gene. *Molecular and Cellular Endocrinology*, *474*, 260–271.

97. Liu, Y., Zhou, X., Xiao, Y., Li, C., Huang, Y., Guo, Q., Su, T., Fu, L., & Luo, L. (2020). miR-188 promotes liver steatosis and insulin resistance via the autophagy pathway. *Journal of Endocrinology*, *245*(3), 411–423.

98. Chen, Y.-J., Chueh, L.-Y., Lee, S.-Y., Ma, P.-F., Chen, P.-C., & Hsu, S. (2021). Coordinated regulation of miR-27 by insulin/CREB/hippo contributes to insulin resistance. *Cellular Signalling*, *81*, 109930.

99. Dai, L.-L., Li, S.-D., Ma, Y.-C., Tang, J.-R., Lv, J.-Y., Zhang, Y.-Q., Miao, Y.-L., Ma, Y.-Q., Li, C.-M., Chu, Y.-Y., et al. (2019). MicroRNA-30b regulates insulin sensitivity by targeting SERCA2b in non-alcoholic fatty liver disease. *Liver International*, *39*(8), 1504–1513.

100. Azzimato, V., Chen, P., Barreby, E., Morgantini, C., Levi, L., Vankova, A., Jager, J., Sulen, A., Diotallevi, M., Shen, J. X., et al. (2021). Hepatic miR-144 drives fumarase activity preventing NRF2 activation during obesity. *Gastroenterology*, *161*(6), 1982–1997.

101. Smolka, C., Schlösser, D., Hohnloser, C., Bemtgen, X., Jänich, C., Schneider, L., Martin, J., Pfeifer, D., Moser, M., Hasselblatt, P., et al. (2021). MiR-100 overexpression attenuates high fat diet induced weight gain, liver steatosis, hypertriglyceridemia and development of metabolic syndrome in mice. *Molecular Medicine*, *27*, 1–18.

102. Wang, X.-Y., Lu, L.-J., Li, Y.-M., & Xu, C.-F. (2022). MicroRNA-376b-3p ameliorates nonalcoholic fatty liver disease by targeting FGFR1 and regulating lipid oxidation in hepatocytes. *Life Sciences*, *308*, 120925.

103. Xu, H., Tian, Y., Tang, D., Zou, S., Liu, G., Song, J., Zhang, G., Du, X., Huang, W., He, B., et al. (2021). An endoplasmic reticulum stress–MicroRNA-26a feedback circuit in NAFLD. *Hepatology*, *73*(4), 1327–1345.

104. Wang, J.-J., Zhang, Y.-T., Tseng, Y. J., & Zhang, J. (2019). miR-222 targets ACOX1, promotes triglyceride accumulation in hepatocytes. *Hepatobiliary & Pancreatic Diseases International*, *18*(4), 360–365.

105. Xu, Z.-X., Li, J.-Z., Li, Q., Xu, M.-Y., & Li, H.-Y. (2022). CircRNA608-microRNA222-PINK1 axis regulates the mitophagy of hepatic stellate cells in NASH related fibrosis. *Biochemical and Biophysical Research Communications*, *610*, 35–42.

106. Li, K., Zhao, B., Wei, D., Wang, W., Cui, Y., Qian, L., & Liu, G. (2020). miR-146a improves hepatic lipid and glucose metabolism by targeting MED1. *International Journal of Molecular Medicine*, *45*(2), 543–555.

107. Du, J., Niu, X., Wang, Y., Kong, L., Wang, R., Zhang, Y., Zhao, S., & Nan, Y. (2015). MiR-146a-5p suppresses activation and proliferation of hepatic stellate cells in nonalcoholic fibrosing steatohepatitis through directly targeting Wnt1 and Wnt5a. *Scientific Reports*, *5*(1), 16163.

108. Li, Y., Luan, Y., Li, J., Song, H., Li, Y., Qi, H., Sun, B., Zhang, P., Wu, X., Liu, X., et al. (2020). Exosomal miR-199a-5p promotes hepatic lipid accumulation by modulating MST1 expression and fatty acid metabolism. *Hepatology International*, *14*, 1057–1074.

109. Ding, J., Xia, C., Cen, P., Li, S., Yu, L., Zhu, J., & Jin, J. (2022). MiR-103-3p promotes hepatic steatosis to aggravate nonalcoholic fatty liver disease by targeting of ACOX1. *Molecular Biology Reports*, *49*(8), 7297–7305.

110. Sun, H., Seok, S., Jung, H., Kemper, B., & Kemper, J. K. (2022). Obesity-induced miR-802

directly targets AMPK and promotes nonalcoholic steatohepatitis in mice. *Molecular Metabolism*, *66*, 101603.

111. Gong, R., Lv, X., & Liu, F. (2018). MiRNA-17 encoded by the miR-17-92 cluster increases the potential for steatosis in hepatoma cells by targeting CYP7A1. *Cellular & Molecular Biology Letters*, *23*, 1–11.

112. Hanin, G., Yayon, N., Tzur, Y., Haviv, R., Bennett, E. R., Udi, S., Krishnamoorthy, Y. R., Kotsiliti, E., Zangen, R., Efron, B., et al. (2018). miRNA-132 induces hepatic steatosis and hyperlipidaemia by synergistic multitarget suppression. *Gut*, *67*(6), 1124–1134.

113. Chu, K., & Gu, J. (2022). microRNA-103a-3p promotes inflammation and fibrosis in nonalcoholic fatty liver disease by targeting HBP1. *Immunopharmacology and Immunotoxicology*, *44*(6), 993–1003.

114. Quezada, H., Guzmán-Ortiz, A. L., Díaz-Sánchez, H., Valle-Rios, R., & Aguirre-Hernández, J. (2017). Omics-based biomarkers: Current status and potential use in the clinic. *Boletín Médico Del Hospital Infantil de México (English Edition)*, *74*(3), 219–226.

115. Organization, W. H. et al. (2001). *Biomarkers in risk assessment: Validity and validation*. World Health Organization.

116. Strimbu, K., & Tavel, J. A. (2010). What are biomarkers? *Current Opinion in HIV and AIDS*, *5*(6), 463–466.

117. Group, B. D. W., Atkinson Jr, A. J., Colburn, W. A., DeGruttola, V. G., DeMets, D. L., Downing, G. J., Hoth, D. F., Oates, J. A., Peck, C. C., Schooley, R. T., et al. (2001). Biomarkers and surrogate endpoints: Preferred definitions and conceptual framework. *Clinical Pharmacology & Therapeutics*, *69*(3), 89–95.

118. Heyn, G., Correa, L., & Magalhaes, K. (2020). The impact of adipose tissue-derived mirnas in metabolic syndrome, obesity, and cancer. Front endocrinol (lausanne). 2020; 11: 563816. *PubMed: Https://Pubmed. Ncbi. Nlm. Nih. Gov/33123088*.

119. Carpi, S., Daniele, S., Almeida, J. F. M. de, & Gabbia, D. (2024). Recent advances in miRNA-based therapy for MASLD/MASH and MASH-associated HCC. *International Journal of Molecular Sciences*, *25*(22), 12229.

120. Gareev, I., Beylerli, O., Yang, G., Sun, J., Pavlov, V., Izmailov, A., Shi, H., & Zhao, S. (2020). The current state of MiRNAs as biomarkers and therapeutic tools. *Clinical and Experimental Medicine*, *20*, 349–359.

121. A. McGregor, R., & S. Choi, M. (2011). microRNAs in the regulation of adipogenesis and obesity. *Current Molecular Medicine*, *11*(4), 304–316.

122. Schwarzenbach, H., Nishida, N., Calin, G. A., & Pantel, K. (2014). Clinical relevance of circulating cell-free microRNAs in cancer. *Nature Reviews Clinical Oncology*, *11*(3), 145–156.

123. Roy, B., Ghose, S., & Biswas, S. (2022). Therapeutic strategies for miRNA delivery to reduce hepatocellular carcinoma. *Seminars in Cell & Developmental Biology*, *124*, 134–144.

124. Torres-Perez, E., Valero, M., Garcia-Rodriguez, B., Gonzalez-Irazabal, Y., Calmarza, P., Calvo-Ruata, L., Ortega, C., Garcia-Sobreviela, M. P., Sanz-Paris, A., Artigas, J. M., et al. (2015). The FAT expandability (FATe) project: Biomarkers to determine the limit of expansion and the complications of obesity. *Cardiovascular Diabetology*, *14*, 1–8.

125. Kleiner, D. E., Brunt, E. M., Van Natta, M., Behling, C., Contos, M. J., Cummings, O. W., Ferrell, L. D., Liu, Y.-C., Torbenson, M. S., Unalp-Arida, A., et al. (2005). Design and validation of a histological scoring system for nonalcoholic fatty liver disease. *Hepatology*, *41*(6), 1313–1321.

126. Peltzer, A., Trigila, A., Pantano, L., Ewels, P., Wang, C., Espinosa-Carrasco, J., Schcolnicov, N., Mohr, C., bot, nf-core, Menden, K., Patel, H., Sturm, G., CKComputomics, Cabus, L., Keys, K. L., Guizard, S., Garcia, M. U., Syme, R., Talbot, A., . . . Tommaso, P. D. (2024). *Nf-core/smrnaseq: v2.4.0 - 2024-10-14 - gray zinc dalmation patch*. Zenodo. https://doi.org/10.5281/ZENODO.

3456879

127. Ewels, P. A., Peltzer, A., Fillinger, S., Patel, H., Alneberg, J., Wilm, A., Garcia, M. U., Di Tommaso, P., & Nahnsen, S. (2020). The nf-core framework for community-curated bioinformatics pipelines. *Nature Biotechnology*, *38*(3), 276–278.

128. Andrews, S. et al. (2010). *FastQC: A quality control tool for high throughput sequence data*. Cambridge, United Kingdom.

129. Chen, S., Zhou, Y., Chen, Y., & Gu, J. (2018). Fastp: An ultra-fast all-in-one FASTQ preprocessor. *Bioinformatics*, *34*(17), i884–i890.

130. Kang, W., Eldfjell, Y., Fromm, B., Estivill, X., Biryukova, I., & Friedländer, M. R. (2018). miRTrace reveals the organismal origins of microRNA sequencing data. *Genome Biology*, *19*, 1–15.

131. Langmead, B., Trapnell, C., Pop, M., & Salzberg, S. L. (2009). Ultrafast and memory-efficient alignment of short DNA sequences to the human genome. *Genome Biology*, *10*, 1–10.

132. Danecek, P., Bonfield, J. K., Liddle, J., Marshall, J., Ohan, V., Pollard, M. O., Whitwham, A., Keane, T., McCarthy, S. A., Davies, R. M., & Li, H. (2021). Twelve years of SAMtools and BCFtools. *GigaScience*, *10*(2). https://doi.org/10.1093/gigascience/giab008

133. Desvignes, T., Loher, P., Eilbeck, K., Ma, J., Urgese, G., Fromm, B., Sydes, J., Aparicio-Puerta, E., Barrera, V., Espin, R., et al. (2020). Unification of miRNA and isomiR research: The mirGFF3 format and the mirtop API. *Bioinformatics*, *36*(3), 698–703.

134. Ewels, P., Magnusson, M., Lundin, S., & Käller, M. (2016). MultiQC: Summarize analysis results for multiple tools and samples in a single report. *Bioinformatics*, *32*(19), 3047. https://doi.org/10.1093/bioinformatics/btw354

135. Wickham, H. (2016). *ggplot2: Elegant graphics for data analysis*. Springer-Verlag New York. https://ggplot2.tidyverse.org

136. R Core Team. (2024). *R: A language and environment for statistical computing*. R Foundation for Statistical Computing. https://www.R-project.org/

137. Posit team. (2023). *RStudio: Integrated development environment for r*. Posit Software, PBC. http://www.posit.co/

138. Wickham, H., Averick, M., Bryan, J., Chang, W., McGowan, L. D., François, R., Grolemund, G., Hayes, A., Henry, L., Hester, J., Kuhn, M., Pedersen, T. L., Miller, E., Bache, S. M., Müller, K., Ooms, J., Robinson, D., Seidel, D. P., Spinu, V., . . . Yutani, H. (2019). Welcome to the tidyverse. *Journal of Open Source Software*, *4*(43), 1686. https://doi.org/10.21105/joss.01686

139. Pantano, L., & Escaramis, G. (2024). *isomiRs: Analyze isomiRs and miRNAs from small RNA-seq*. https://doi.org/10.18129/B9.bioc.isomiRs

140. Love, M. I., Huber, W., & Anders, S. (2014). Moderated estimation of fold change and dispersion for RNA-seq data with DESeq2. *Genome Biology*, *15*, 550. https://doi.org/10.1186/s13059-014-0550-8

141. Carlson, M. (2024). *Org.hs.eg.db: Genome wide annotation for human*.

142. Ru, Y., Kechris, K. J., Tabakoff, B., Hoffman, P., Radcliffe, R. A., Bowler, R., Mahaffey, S., Rossi, S., Calin, G. A., Bemis, L., & Theodorescu, D. (2014). The multiMiR r package and database: Integration of microRNA target interactions along with their disease and drug associations. *Nucleic Acids Research*, *42*(17), e133. https://doi.org/10.1093/nar/gku631

143. Ru, Y., Mulvahill, M., Mahaffey, S., & Kechris, K. (n.d.). *multiMiR: Integration of multiple microRNA-target databases with their disease and drug associations*. https://github.com/KechrisLab/multiMiR

144. Tenenbaum, D., & Maintainer, B. P. (2024). *KEGGREST: Client-side REST access to the kyoto encyclopedia of genes and genomes (KEGG)*. https://doi.org/10.18129/B9.bioc.KEGGREST

145. Gómez-Lechón, M. J., Donato, M. T., Martínez-Romero, A., Jiménez, N., Castell, J. V., &

O'Connor, J.-E. (2007). A human hepatocellular in vitro model to investigate steatosis. *Chemico-Biological Interactions*, *165*(2), 106–116.

146. Belfort, R., Harrison, S. A., Brown, K., Darland, C., Finch, J., Hardies, J., Balas, B., Gastaldelli, A., Tio, F., Pulcini, J., et al. (2006). A placebo-controlled trial of pioglitazone in subjects with nonalcoholic steatohepatitis. *New England Journal of Medicine*, *355*(22), 2297–2307.

147. Rao, X., Huang, X., Zhou, Z., & Lin, X. (2013). An improvement of the 2^ (−delta delta CT) method for quantitative real-time polymerase chain reaction data analysis. *Biostatistics, Bioinformatics and Biomathematics*, *3*(3), 71.

148. Love, M. I., Huber, W., & Anders, S. (2014). Moderated estimation of fold change and dispersion for RNA-seq data with DESeq2. *Genome Biology*, *15*, 1–21.

149. Chrysavgis, L., & Cholongitas, E. (2024). From NAFLD to MASLD: What does it mean? In *Expert Review of Gastroenterology & Hepatology* (6; Vol. 18, pp. 217–221). Taylor & Francis.

150. Jin, X., Chen, Y., Kong, M., Zheng, L., Yang, Y., & Li, Y. (2012). Transition from hepatic steatosis to steatohepatitis: Unique microRNA patterns and potential downstream functions and pathways. *Journal of Gastroenterology and Hepatology*, *27*(2), 331–340.

151. Cotter, T. G., & Rinella, M. (2020). Nonalcoholic fatty liver disease 2020: The state of the disease. *Gastroenterology*, *158*(7), 1851–1864.

152. Kloting, N., Berthold, S., Kovacs, P., Schon, M. R., Fasshauer, M., Ruschke, K., Stumvoll, M., & Bluher, M. (2009). MicroRNA expression in human omental and subcutaneous adipose tissue. *PloS One*, *4*(3), e4699.

153. Liu, C.-H., Ampuero, J., Gil-Gómez, A., Montero-Vallejo, R., Rojas, Á., Muñoz-Hernández, R., Gallego-Durán, R., & Romero-Gómez, M. (2018). miRNAs in patients with non-alcoholic fatty liver disease: A systematic review and meta-analysis. *Journal of Hepatology*, *69*(6), 1335–1348.

154. Liu, X.-L., Pan, Q., Zhang, R.-N., Shen, F., Yan, S.-Y., Sun, C., Xu, Z.-J., Chen, Y.-W., & Fan, J.-G. (2016). Disease-specific miR-34a as diagnostic marker of non-alcoholic steatohepatitis in a chinese population. *World Journal of Gastroenterology*, *22*(44), 9844.

155. Szabo, G., & Csak, T. (2016). Role of MicroRNAs in NAFLD/NASH. *Digestive Diseases and Sciences*, *61*, 1314–1324.

156. Tobaruela-Resola, A. L., Riezu-Boj, J. I., Milagro, F. I., Mogna-Pelaez, P., Herrero, J. I., Elorz, M., Benito-Boillos, A., Tur, J. A., Martínez, J. A., Abete, I., et al. (2024). Multipanel approach including miRNAs, inflammatory markers, and depressive symptoms for metabolic dysfunction-associated steatotic liver disease diagnosis during 2-year nutritional intervention. *Nutrients*, *16*(11), 1547.

157. Tobaruela-Resola, A. L., Milagro, F. I., Elorz, M., Benito-Boillos, A., Herrero, J. I., Mogna-Peláez, P., Tur, J. A., Martínez, J. A., Abete, I., & Zulet, M. Á. (2024). Circulating miR-122-5p, miR-151a-3p, miR-126-5p and miR-21-5p as potential predictive biomarkers for metabolic dysfunction-associated steatotic liver disease assessment. *Journal of Physiology and Biochemistry*, 1–14.

158. Catanzaro, G., Filardi, T., Sabato, C., Vacca, A., Migliaccio, S., Morano, S., & Ferretti, E. (2021). Tissue and circulating microRNAs as biomarkers of response to obesity treatment strategies. *Journal of Endocrinological Investigation*, *44*, 1159–1174.

159. Roderburg, C., Urban, G.-W., Bettermann, K., Vucur, M., Zimmermann, H., Schmidt, S., Janssen, J., Koppe, C., Knolle, P., Castoldi, M., et al. (2011). Micro-RNA profiling reveals a role for miR-29 in human and murine liver fibrosis. *Hepatology*, *53*(1), 209–218.

160. Ludwig, N., Leidinger, P., Becker, K., Backes, C., Fehlmann, T., Pallasch, C., Rheinheimer, S., Meder, B., Stähler, C., Meese, E., et al. (2016). Distribution of miRNA expression across human tissues. *Nucleic Acids Research*, *44*(8), 3865–3877.

161. Thomou, T., Mori, M. A., Dreyfuss, J. M., Konishi, M., Sakaguchi, M., Wolfrum, C., Rao, T. N.,

Winnay, J. N., Garcia-Martin, R., Grinspoon, S. K., et al. (2017). Adipose-derived circulating miRNAs regulate gene expression in other tissues. *Nature*, *542*(7642), 450–455.

162. Fan, J., Zhang, J., Huang, S., & Li, P. (2020). lncRNA OSER1-AS1 acts as a ceRNA to promote tumorigenesis in hepatocellular carcinoma by regulating miR-372-3p/Rab23 axis. *Biochemical and Biophysical Research Communications*, *521*(1), 196–203.

163. Syring, I., Bartels, J., Holdenrieder, S., Kristiansen, G., Müller, S. C., & Ellinger, J. (2015). Circulating serum miRNA (miR-367-3p, miR-371a-3p, miR-372-3p and miR-373-3p) as biomarkers in patients with testicular germ cell cancer. *The Journal of Urology*, *193*(1), 331–337.

164. Murray, M. J., Huddart, R. A., & Coleman, N. (2016). The present and future of serum diagnostic tests for testicular germ cell tumours. *Nature Reviews Urology*, *13*(12), 715–725.

165. Wang, Q., Liu, S., Zhao, X., Wang, Y., Tian, D., & Jiang, W. (2017). MiR-372-3p promotes cell growth and metastasis by targeting FGF 9 in lung squamous cell carcinoma. *Cancer Medicine*, *6*(6), 1323–1330.

166. Xu, S.-Y., Xu, P.-F., & Gao, T.-T. (2018). MiR-372-3p inhibits the growth and metastasis of osteosarcoma cells by targeting FXYD6. *European Review for Medical & Pharmacological Sciences*, *22*(1).

167. Majdalawieh, A., Zhang, L., Fuki, I. V., Rader, D. J., & Ro, H.-S. (2006). Adipocyte enhancer-binding protein 1 is a potential novel atherogenic factor involved in macrophage cholesterol homeostasis and inflammation. *Proceedings of the National Academy of Sciences*, *103*(7), 2346–2351.

168. Gerhard, G. S., Hanson, A., Wilhelmsen, D., Piras, I. S., Still, C. D., Chu, X., Petrick, A. T., & DiStefano, J. K. (2019). AEBP1 expression increases with severity of fibrosis in NASH and is regulated by glucose, palmitate, and miR-372-3p. *PloS One*, *14*(7), e0219764.

169. Zeng, G., Liu, X., Zheng, Z., Zhao, J., Zhuo, W., Bai, Z., Lin, E., Cai, S., Cai, C., Li, P., et al. (2024). Knockdown of RASD1 improves MASLD progression by inhibiting the PI3K/AKT/mTOR pathway. *Lipids in Health and Disease*, *23*(1), 424.

170. Riaz, F., Chen, Q., Lu, K., Osoro, E. K., Wu, L., Feng, L., Zhao, R., Yang, L., Zhou, Y., He, Y., et al. (2021). Inhibition of miR-188-5p alleviates hepatic fibrosis by significantly reducing the activation and proliferation of HSCs through PTEN/PI3K/AKT pathway. *Journal of Cellular and Molecular Medicine*, *25*(8), 4073–4087.

171. Thamjamrassri, P. (2022). *Exploring roles of MiR-372-3p in proliferation of hepatocellular carcinoma cells*.

172. Kazemzadeh, R., Kheirollahi, M., Mard, S. A., Ahangarpour, A., & Savari, F. (2024). Regulatory, diagnostic, and therapeutic roles of microRNAs in chronic liver diseases. *Acta Gastro-Enterologica Belgica*, *87*.

173. Sun, J., Shi, R., Zhao, S., Li, X., Lu, S., Bu, H., Ma, X., & Su, C. (2017). E2F8, a direct target of miR-144, promotes papillary thyroid cancer progression via regulating cell cycle. *Journal of Experimental & Clinical Cancer Research*, *36*, 1–14.

174. RNAcentral: A comprehensive database of non-coding RNA sequences. (2017). *Nucleic Acids Research*, *45*(D1), D128–D134.

175. Rowe, M. M., & Kaestner, K. H. (2023). The role of non-coding RNAs in liver disease, injury, and regeneration. *Cells*, *12*(3), 359.

176. Kooshkaki, O., Rezaei, Z., Rahmati, M., Vahedi, P., Derakhshani, A., Brunetti, O., Baghbanzadeh, A., Mansoori, B., Silvestris, N., & Baradaran, B. (2020). MiR-144: A new possible therapeutic target and diagnostic/prognostic tool in cancers. *International Journal of Molecular Sciences*, *21*(7), 2578.

177. Zhao, J., Li, H., Zhao, S., Wang, E., Zhu, J., Feng, D., Zhu, Y., Dou, W., Fan, Q., Hu, J., et al. (2021). Epigenetic silencing of miR-144/451a cluster contributes to HCC progression via

paracrine HGF/MIF-mediated TAM remodeling. *Molecular Cancer*, *20*, 1–16.

178. Ye, Z., Cheng, M., Fan, L., Ma, J., Zhang, Y., Gu, P., Xie, Y., You, X., Zhou, M., Wang, B., et al. (2023). Plasma microRNA expression profiles associated with zinc exposure and type 2 diabetes mellitus: Exploring potential role of miR-144-3p in zinc-induced insulin resistance. *Environment International*, *172*, 107807.

179. Niitsu, Y., Komiya, C., Takeuchi, A., Hara, K., Horino, M., Aoki, J., Okazaki, R., Murakami, M., Tsujimoto, K., Ikeda, K., et al. (2023). Increased serum extracellular vesicle miR-144-3p and miR-486a-3p in a mouse model of adipose tissue regeneration promote hepatocyte proliferation by targeting txnip. *Plos One*, *18*(5), e0284989.

180. Kennedy, L., Meadows, V., Sybenga, A., Demieville, J., Chen, L., Hargrove, L., Ekser, B., Dar, W., Ceci, L., Kundu, D., et al. (2021). Mast cells promote nonalcoholic fatty liver disease phenotypes and microvesicular steatosis in mice fed a western diet. *Hepatology*, *74*(1), 164–182.

181. Lin, W., Wen, X., Li, X., Chen, L., Wei, W., Zhang, L., & Chen, J. (2022). MiR-144 regulates adipogenesis by mediating formation of c/EBPα-FOXO1 protein complex. *Biochemical and Biophysical Research Communications*, *612*, 126–133.

182. Ramadan, N. M., Elmasry, K., Elsayed, H. R. H., El-Mesery, A., & Eraky, S. M. (2022). The hepatoprotective effects of n3-polyunsaturated fatty acids against non-alcoholic fatty liver disease in diabetic rats through the FOXO1/PPARα/GABARAPL1 signalling pathway. *Life Sciences*, *311*, 121145.

183. Cao, T., Li, H., Hu, Y., Ma, D., & Cai, X. (2014). miR-144 suppresses the proliferation and metastasis of hepatocellular carcinoma by targeting E2F3. *Tumor Biology*, *35*, 10759–10764.

184. Pu, C., Huang, H., Wang, Z., Zou, W., Lv, Y., Zhou, Z., Zhang, Q., Qiao, L., Wu, F., & Shao, S. (2018). Extracellular vesicle-associated mir-21 and mir-144 are markedly elevated in serum of patients with hepatocellular carcinoma. *Frontiers in Physiology*, *9*, 930.